NASA Contractor Report 187580

INFLATED CONCEPTS FOR THE EARTH SCIENCE GEOSTATIONARY PLATFORM AND AN ASSOCIATED FLIGHT EXPERIMENT

G. Friese

L'GARDE, INC.
Tustin, California

Contract NAS1-18681
January 1992

National Aeronautics and
Space Administration

Langley Research Center
Hampton, Virginia 23665-5225

FOREWORD

This program was performed for the National Aeronautics and Space Administration; Langley Research Center. Guidance was provided by Messrs. Tom Campbell and Lenwood Clark of the NASA-Langley Research Center, and it is gratefully acknowledged. Within L'Garde, Dr. Costa Cassapakis was Program Manager, and Gil Friese was Program Engineer. Program contributions were made by Dr. Dave Chittenden, Tom Daggett, Dr. Koorosh Gidanian, Evie Gilbert, Anne Handberry, Rhonda Nelson, Dr. Art Palisoc, Dr. Mitch Thomas, Chris Thompson and Geoff Williams.

Proprietary thin films discussed in this report include Mylar®, Tedlar®, Dartek® and Kapton®. These are all trade names owned by E.I. duPont De Nemours and Company, Wilmington, Delaware.

TABLE OF CONTENTS

LIST OF TABLES

LIST OF ILLUSTRATIONS

Figure | Page

1.0 INTRODUCTION

Large parabolic reflectors and solar concentrators are of great interest for microwave transmission, solar powered rockets and earth observations. Collector subsystems have been under slow development for about a decade. Inflated paraboloids have a great weight and package volume advantage over mechanically erected systems, and therefore have been receiving greater attention recently.

The objective of this program was to produce a "conceptual definition of an experiment to assess in-space structural damping characteristics and effects of the space meteoroid environment upon structural integrity and service life of large inflatable structures."

Three major areas concerning inflatables were ultimately studied under this program.

Earth Science Geostationary platform (ESGP)

The flight experiment was to have been based upon an inflatable solar concentrator. However, much of the work to be done on this program for inflatable solar concentrators was being done on other programs. Therefore, to avoid redundancy, the Earth Science Geostationary Platform (ESGP) was selected as an alternate baseline, and an inflatable ESGP was conceived to help define the experiment.

The ESGP inflated concept is described in Section 2.0 along with studies performed to support concept definition. The ESGP is to operate at frequencies up to 60 GHz. Three meter diameter inflatable paraboloids have been demonstrated on the ground to have sufficient accuracy to support frequencies up to about 10 GHz (Section 2.3). Therefore, the ESGP inflated concept is a hybrid in which a small rigid paraboloid (4.2m diameter) is used at the higher frequencies where paraboloid size can be small, and an inflated paraboloid (28m diameter) is used at the lower frequencies where a large dish is essential.

The ESGP inflated paraboloid consists of the 28m off-axis reflector, its support structure, and the inflation mechanisms/sensors including the inflation gas required for a five year life. The total weight is 180 kg, and its package (launch) volume is 0.5 cubic meters. If the support structure is extended to include that necessary to connect together the large reflector, sub-reflector and feed array, another 195 kg of weight and 1.2 cubic meter of package volume is necessary.

Flight Experiment

The ESGP concept was the basis for the flight experiment described in Section 3.0. The test results would be applicable to any large space paraboloid. The flight experiment payload would be placed into orbit above 400kms perigee. In-space structural damping characteristics will be determined as required. In addition, paraboloid accuracy is being measured rather than the effects of the space meteoroid environment. Both could be evaluated simultaneously if the experiment were placed in high earth orbit (above 1000 km) where drag is

insignificant. However, most of the opportunities for space flights are for orbits around 400 km -- from which a large, low weight inflatable will de-orbit in less than a day. It is believed that inflated paraboloid accuracy must be demonstrated first.

The flight inflatable is a 28m off-axis paraboloid with full instrumentation and a telemetry system for transmitting the data to earth. Its launch weight is 200 kg and it packages in 0.4 cubic meter.

The prime instrumentation is a video camera and a bank of lights located at the paraboloid's average center of curvature (not at its focal point), which is about 61m from the paraboloid edge. The principle behind this instrumentation is simple. If the reflector were a spherical segment instead of a paraboloid, and a light were located at the radius of curvature of this surface, and the spherical segment viewed by a camera in this same vicinity, a perfect surface would result in a uniformly lit image. Portions of the surface that are in error would show up black (unlit) since the reflected light would be off course. For every pixel lit up on the video image, the slope of the corresponding element of the spherical segment is known with precision. By using a bank of lights, the surface of a paraboloid can be accurately reconstructed post-test. Each light would be turned on for about a second when all the other lights are off. Every pixel on the video screen relates to small area on the paraboloid. If that pixel is lit (i.e., white), then the slope of that piece of paraboloid is known. When another light is turned on instead, the slopes of another set of paraboloid areas will be known. Given sufficient lights and a paraboloid of reasonable accuracy, the paraboloid surface can be reconstructed from the video data, and its accuracy calculated. This technique was developed and successfully used by McDonnell Douglas for ground test of solar concentrators.

The flight experiment was scheduled so as to fly about 5.3 years after go-ahead at a cost of approximately $5M (plus government launch costs).

Meteoroids

As mentioned earlier, the effects of meteoroids will not be determined in this flight experiment. Instead, NASA's meteoroid models, NASA and L'Garde hypervelocity test data and L'Garde analyses were joined to produce the meteoroid model reported in Section 4.0. Meteoroid damage (i.e., holes in the inflatable's thin film) is more severe than formerly expected, but still low enough to make space inflatables practical. It had been assumed that a meteoroid produced drilled holes in both inflatable films that were about the same size as the meteoroid. However, test data now show that the total hole area in the films is greater than this. For most large space inflatables, the lowest weight approach is to use the thinnest film available so that both required internal pressure and first film meteoroid damage are minimized, and to construct thin film meteoroid shields inside the inflatable to protect the second inflatable film from meteoroid damage. Such shields are low in weight, and weigh less than the additional inflatant that would have to be carried to replace gas lost through holes in the second film.

The Section 4.0 meteoroid damage model makes use of all available test data for thin films, and analysis where there is no test data. Considerably more ground test data is needed for both high and low film thickness/particle diameter ratio regions. The model, however, is believed to be conservative; that is, it predicts more damage than what will occur because of the simplifying assumptions used.

2.0 EARTH SCIENCE GEOSTATIONARY PLATFORM INFLATED SUBSYSTEM CONCEPT

NASA provided the basic dimensions and locations of the reflector, sub-reflector, and feed array for their Earth Science Geostationary Platform (ESGP). An inflated ESGP concept was generated using this information and inflatables technology. Section 2.1 describes the concept. The reflector and structure weigh about 375 kg and will occupy about 1.7 cubic meters of space in the launch vehicle -- exclusive of the sub-reflector, feed array and the electrical equipment needed to operate the ESGP following erection.

There was additional work done in support of this concept in the areas of thin films, surface accuracy, and heat transfer. These efforts are summarized in Sections 2.2 through 2.4, respectively.

2.1 CONCEPT DESCRIPTION

The inflated ESGP is shown in Figure 1. The main reflector is a 28m inflatable off-axis paraboloid with a 4.2m rigid parabolic mirror at its center. The use of the inflatable antenna in conjunction with a smaller precision structure provides both the large diameter needed for high resolution at lower frequencies (<10GHz) (see Section 2.3) and the thermal stability needed for the enclosed precision structure at short wavelengths (See Section 2.4).

The sub-reflector (upper right hand corner of Figure 1) is shown as an erectable rose petal type of mirror. An inflatable may not be competitive for this application because of the sub-reflector's minimum radius of curvature which is believed to be ten meters. The pressure required to provide sufficient stress in the reflector material is about 3.2 Pa. At this pressure, it is estimated that about 70 kg of gas is needed to replace that lost through holes produced by meteoroids over a five year period.

The sub-reflector is guided by four initially inflated, self-rigidizing guide rails. The hardware attaching the sub-reflector to the guide rails includes a mechanism to make adjustments in sub-reflector position, especially since the guide rails are not precision items.

The pivoting feed array, also rigid, is mounted on a honeycomb (or a similar stiff, low weight panel). The feed, sub-reflector and reflector are held in position by self-rigidizing cylinders, a cross-section of which is shown in Section A-A of Figure 1. The ESGP must be in high earth orbit to avoid being de-orbited by drag, and to avoid the debris that exists in low earth orbit.

2.1.1 Inflated Reflector Subsystem

The antenna dish is made of 7.6 micron Kapton® film metallized with aluminum. The cover is the same thin film but non-metallized. For the purposes of this point design, Kapton® was used because of its known survivability in space, but other films may be superior. Section 2.2.3 describes some film testing that was conducted on this program. In particular, the films were tested to determine if their properties would allow lower pressures and therefore lower replacement inflatant requirements. Thin film survivability and other requirements are addressed in Section 2.2.

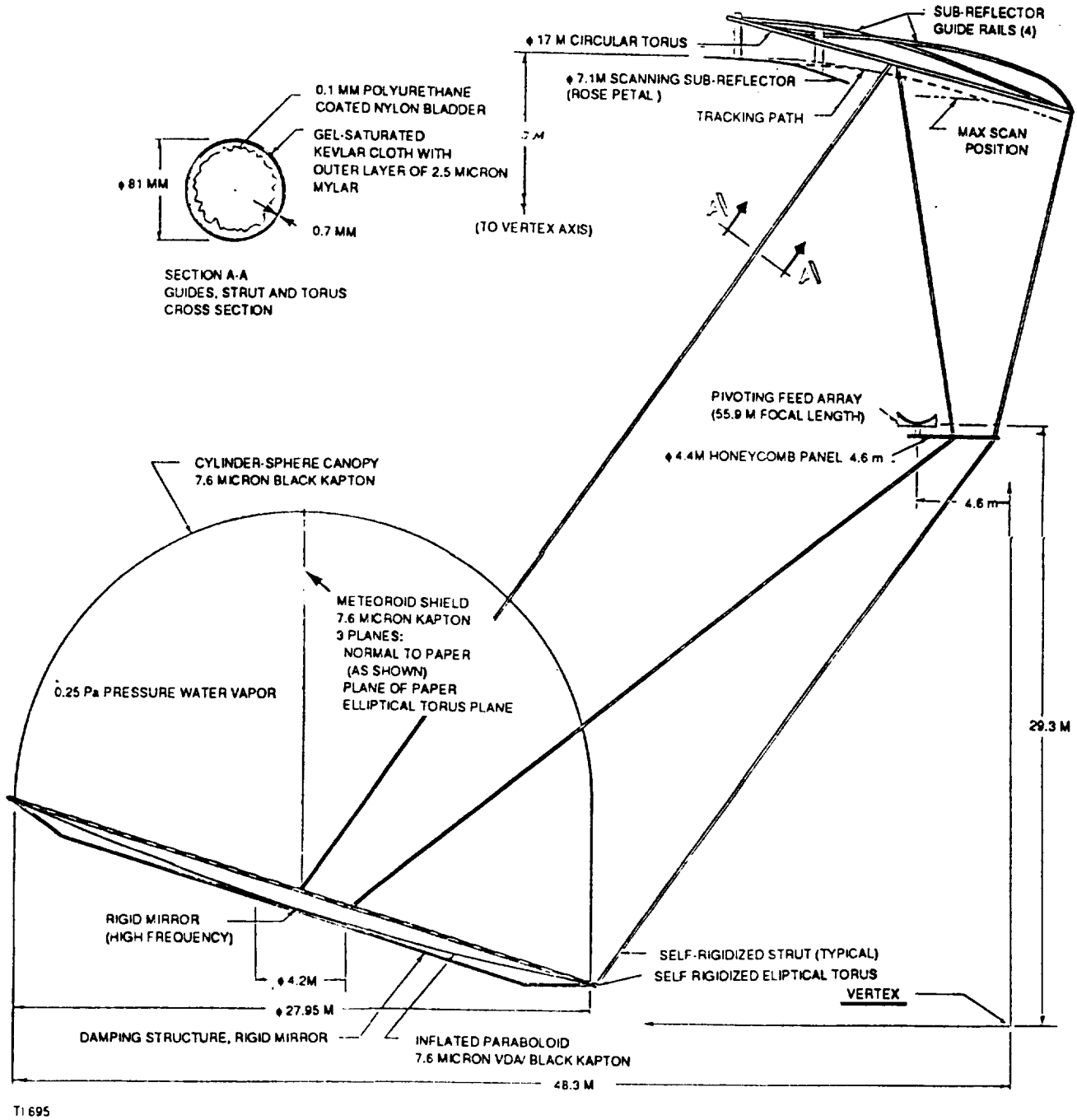

Figure 1. Earth Science Geostationary Platform (ESGP)

The 28 meter off-axis reflector is made from 24 gores of thin film that may be as wide as 1.2 meters. Each gore has a slightly different flat pattern, mainly where it interfaces with the torus. Gores are precision cut, butt jointed, and attached to each other by bonding 24 mm wide tape of the same material to them with a flexible adhesive.

The collector obtains its accuracy by the use of properly shaped gores, and the correct pressure. The gores are designed and built so that they form a three-dimensional, approximately parabolic shape after they are bonded together. Without pressure, however, the gores would not have the double curvatures needed for accuracy at the higher frequencies; that is, the collector would look somewhat like an umbrella. The pressure basically strains each gore until the length of its centerline equals the length of its edge.

The internal pressure (0.25 Pa) was selected to produce a skin stress of 2.1 MPa in the parabolic reflector. This stress level should pull most of the packaging wrinkles out of the thin film. Given this pressure and the maximum available film width of 1.5 meters, the gore flat pattern can be designed such that it will form the correct parabolic shape. Past work by L'Garde and others has shown that pressure need only be accurate to within about a factor of two.

The canopy is a cylinder cone shape rather than a mirror image of the paraboloid to reduce the loads in the torus by nearly a factor of two. The extra weight of Kapton® is more than offset by a lesser torus weight. The maximum stress in the canopy is only 0.5 MPa because its radius of curvature is an order of magnitude lower than that of the paraboloid.

The volume within the paraboloid-canopy is 8400 cubic meters. The weight of the water vapor within this space is only 15 grams. The water will not interfere with high frequency radar transmission because there is so little of it. If this density of water vapor were in sea level air at 295K, the relative humidity would be only 0.0002%! (Inflatant selection is summarized in Section 4.4.)

Meteoroid damage is not insignificant. Meteoroids will produce a hole area of approximately 1.2 mm^2 per square meter of projected area during the first year. Make-up gas weight during the first year would be up to 3.3kg. A five year life requires 83 kg of water. The basis for these estimates are provided in Section 4.0. Replacement water would most likely be located in or on the elliptical torus contained by butyl rubber. Butyl rubber has the lowest water vapor permeability of any flexible material yet tested. Another option is to contain the water in rigid container(s) near the pivoting feed array.

2.1.2 SELF-RIGIDIZING STRUCTURE

L'Garde started working on self-rigidizing inflatables over 10 years ago. Originally, aluminum foil was bonded to a thin film, and made into a cylinder. Gas would be used to unfold, erect and stress the structure into a smooth aluminum cylinder. The approach was originally used on the Echo 30 meter spherical satellite in the 50's. The system works and is useable on any space structure where the loads are low.

More recently, Kevlar® cloth was filled with gel and rolled into a cylinder. Saturated with water, the material is flexible and can be packaged.

Gas is used to unfold and erect the structure. The water vaporizes in space leaving an amazingly strong structure.

Cylinders, 81 mm in diameter and 0.7 mm thick, were tested. They resisted 250Nm in bending and 4300N in compression. Modulus of elasticity is 28 GPa -- 40% of that for aluminum. This structure, developed under the Inflatable Structure Technology Program (Reference 2) was used throughout the ESGP concept.

The water must be kept from vaporizing on the ground or prematurely in space. On the ground, the structure will be kept in a container that is reasonably impermeable and leak-free. In space, the structure must be erected before it rigidizes. Calculations indicate that erection will take up to twelve seconds after the gas starts entering the tubes. Therefore, rigidization must be prevented for at least this period. Rigidization can occur prematurely due to water freezing during the vaporization process. Tests and analysis (Reference 2) show that this can be prevented by a semi-permeable sleeve covering the self-rigidizing structure. A 4 micron thin Mylar® sheet would delay rigidization for one hour -- more than enough time -- without any freezing taking place. This film is included in the design concept.

The torus is needed primarily to hold the edges of the paraboloid in place. It must resist the forces produced by the pressure within the paraboloid-canopy. These forces, calculated using work developed earlier (Reference 1), are shown in Figure 2. The peak loads are 215N compression and 145Nm bending moment per L'Garde tests. The selected torus structure was tested under another program and was found to take 4300N compression or 250Nm bending. If the conventional elastic buckling approach is used, applied load is 63% of ultimate:

$$\frac{215}{4300} + \frac{145}{250} = 63\%$$

The loads in the struts are unknown, but close to zero. The self-rigidizing structure is overly strong for this application, but is used to give a worst case weight. A weaker lower weight self-rigidizing gel sub-system could be developed for the struts, if necessary.

2.1.3 Weight and Package Volume

The weight and package volume breakdown of the ESGP is shown in Table 1. These are launch weights because they include the water for the self-rigidizing structure. After rigidization, the structure (struts, tori, guide rails) would weigh 17% less.

Package volume calculations for the inflatable items were performed assuming that they could be packaged with only 20% efficiency. The inflated structure must be kept in a reasonably impermeable container to prevent premature water vaporization. Actually two containers are indicated, one on each side of the honeycomb platform. These two containers would be connected to allow the two long struts to occupy both containers. Everything weighed in Table 1 would be inside these containers except for inflation tanks and hardware. The honeycomb panel which would form one side of both containers.

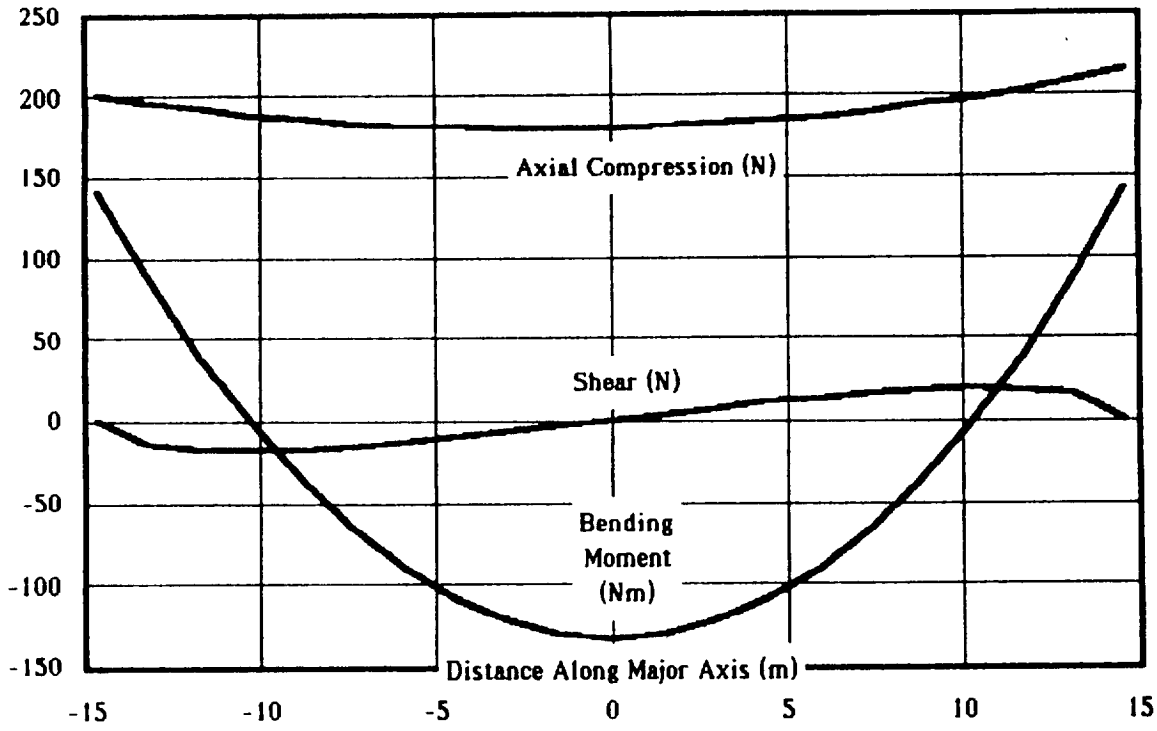

Figure 2. Elliptical Torus Loads

2.2 THIN FILMS

For precision collectors used in space, films 8 to 25 microns in thickness are used. There are many films from which to select and also many requirements that need to be met by a film for any particular mission. Section 2.2.1 contains general thin film requirements for most large collectors and other inflatables. Section 2.2.2 contains a summary of literature research that was conducted to determine the effects of the space environment on thin films. Included are suggestions for the best films to be used in space. Section 2.2.3 summarizes a small test effort to evaluate films that have not been previously used by L'Garde.

2.2.1 General Considerations

There are numerous requirements for an inflatable parabolic reflector. In general, all of the following can be met with available films.

The most basic requirement is a high reflectance in the appropriate wave lengths. For example, in a solar reflector a 90% or greater reflectivity in the most radiant part of the solar spectrum is desired. For a microwave reflector, gaps in the conductive surface must be small relative to the wavelength(s) used.

The reflector surface must also be smooth. For example, the woven pattern of fabrics will tend to produce a more diffuse reflection than wanted for a solar concentrator. Surfaces can be smoothed out by a coating or laminated film, while

TABLE 1. LIFT-OFF WEIGHT (KILOGRAMS)

	Weight (kg)	Package Volume m^3
Paraboloid Subsystem		
Paraboloid	8	0.02
Canopy	14	0.05
Internal Meteoroid Shield	14	0.05
Elliptical Torus	30	0.09
Tori-Paraboloid Interface	14	0.05
Replacement Water (5 Years)	90	0.17
Tanks and Inflation Hardware	10	0.02
Nitrogen Inflatant	0	0.00
	180	0.46
Remaining Structure		
Struts	90	0.27
Circular Torus	18	0.06
Guide Rails	26	0.08
Nitrogen Inflatant	1	0.00
Tank and Inflation Hardware	4	0.07
Inflatable Canister	56	0.77
	195	1.25
Not Weighed		
4.3m Mirror		
Sub-Reflector & Interface		
Feed Array		
Microwave Equipment		
Power		
Microprocessor System		
Communications		
TV Camera		
Guidance		
Reaction Control Subsystems		

retaining a fabric backing for strength. Dust or powder used during packing to prevent sticking of surfaces may cause a degradation of surface smoothness if it remains on the surface of the inflated product.

It must be possible to orient the reflecting surface to direct the radiation to the proper location. The local surface orientation can usually be achieved with an object that holds its proper shape due to inflation pressure, stretching to the appropriate contour when the correct pressure is maintained. Limited data indicate that pressure level does not have to be held with precision.

Materials must have the tensile strength to resist excess deformation, tearing, or puncture during or after inflation. They must resist the extra stresses placed on the edges and corners in a folded inflatable object, which may result in local deformation or stress cracking while the object is in storage.

Thin materials are usually wanted for inflatables so that packaged subsystem mass and volume are low. A space inflatable collector generally has a paraboloid, a supporting torus and replacement gas. The weight of these three items are usually directly proportional to the paraboloid material thickness.

Some electrical conductivity of the surface is needed if the object is to be placed in an environment that causes electrical charge to accumulate unevenly on the surface. Poor conductivity may result in destructive sparking between sections of the spacecraft.

Inflatable spacecraft are generally made of pieces formed to be seamed together and to yield a special shape on inflation. Leak-free and strong seams must be made that will not cause a loss of other properties.

Outgassing by desorption must be limited from the skin material, or the adhesive used in seams, if other spacecraft parts might be contaminated by reabsorption of these vapors. NASA specification SPR-R-0022A requires that materials have a total mass loss no greater than one percent, and a loss of condensible materials less than one tenth percent. Some inflatables need to be heated or placed in a vacuum as part of their manufacture to meet this requirement.

Impermeability to gas pressure is required so that inflated objects remain inflated and retain their desired shape for the expected lifetime.

Thermal expansion may be an important property if it causes temporary or permanent distortion of the reflector's shape, or causes delamination due to differential expansion of a laminant. See Section 2.4.

The film properties must be retained in storage before launch, as well as during the expected lifetime in space. An inflatable object is usually stored in a folded condition. The film will be exposed to local stresses at creases and corners. Creases due to deformation may remain in the inflated object; however, the inflation pressure will largely smooth them out. The number of permanent creases increases with packaging density.

Since all materials have some tendency to absorb water, the humidity of the storage area should be controlled at a low value. Excess humidity might cause material swelling due to absorption, or differential expansion. Micro-organisms are also encouraged to grow by high humidity.

If the material surfaces are improperly painted or printed, these thin deposits may come off in spots and transfer to contact surfaces primarily when densely packaged. Metallized surfaces can oxidize and change color with time in uncontrolled storage.

Vibrations (such as during launch) may wear off parts of the film or surface coating particularly if loosely packaged within a "rough" container.

2.2.2 Space Environment

The literature has been searched for information regarding the effect of the space environment on thin films. A bibliography of reports read but not referenced below is included at the end of this report. The ESGP design concept has not been modified to reflect all of the space environments described below.

Low Earth Orbit (LEO)

The low earth orbit generally is considered to be between 200 and 500 Km, and satellite velocities are about 8Km per second in this orbit.

The most destructive hazard is generally thought to be atomic oxygen. Although the pressure is 1 to 10 microPascal, there are still about 800 million oxygen atoms per cubic centimeter. The spacecraft travelling in orbit crashes against these oxygen atoms at an order of magnitude higher velocity than their thermal velocity causing severe erosion. Materials that are less reactive with oxygen in laboratory experiments are also less eroded by atomic oxygen, indicating a chemical mechanism.

The degradation due to atomic oxygen will depend somewhat on the characteristics of the satellite orbit. For example, Durcanin (Reference 3) states that the atomic oxygen fluence is 1.2 $(10)^{21}$ atoms per sq. cm. per year in the ram direction (for nominal solar activity) for the minimal space station orbital altitude of 460Km. The solar viewing surface of such a satellite will get 57% of such flux. In contrast, for a 98 degree inclination polar orbiting platform, the atomic oxygen fluence is 2.8 $(10E)^{21}$ atoms per sq. cm. per year in the ram direction, with 65% of that on the solar viewing surface. The NASA SINTERS (Surface Interaction Effects Routine) computer model estimates the atomic oxygen fluence on a spacecraft surface given the flight orbital conditions and the predicted solar activity.

Ionizing radiation in orbit includes electrons, X-rays, and gamma rays that are more damaging to organic materials, as well as neutrons and protons that also damage inorganics. The total dose absorbed for a given depth of material can be predicted for an orbit scenario using the SHIELDOSE computer program (Reference 4). For short exposure, ionizing radiation isn't a serious problem in LEO equatorial orbit, but it is far worse in a polar orbit, or an orbit which passes through the South Atlantic anomaly where charged particles from the sun are trapped at 150 to 300Km altitude, and from 0 to 60 degrees West longitude and 20 to 50 degrees South latitude.

Ultraviolet radiation in LEO from the sun is 0.12 to 0.4 micrometers and contains 8.8% of the sun's energy. Polymer films are sensitive to this radiation which may cause chain scission (resulting in lost strength) or cross linking (resulting in increased brittleness). Although UV penetration is perhaps only 100 micrometers in a polymer, critical surface properties may be changed.

Synergistic effects of these hazards make prediction uncertain, and experiments essential. For example:

- UV causes bond scission in polymer films. When the film surface is thus breached, atomic oxygen can cause more destruction. Although Teflon® usually tests very resistant to atomic oxygen, when samples were exposed to UV and simulated atomic oxygen at the same time, Teflon® became no more resistant than an ordinary organic polymer film.

- Similarly, both micrometeoroids and thermal cycling can cause minute breaks in a protective surface that can permit access to the interior for atomic oxygen. The latter then erodes out a void beneath the rest of the protective coating until the edges of the hole are no longer supported, gradually enlarging it.

It must be concluded that there is no substitute for testing materials in the actual environment proposed for exposure. This allows all the potentially destructive effects to work together, and permits unforeseen effects to act.

Prior to the recent recovery of the Long Duration Exposure Facility (LDEF), the longest formal material test in space was only 40 hours. Naturally it is very dangerous to extrapolate such experience to the period of several years proposed for some space missions. Data from the LDEF experiment, when analyzed, will be crucial for future materials decisions.

Geosynchronous Earth Orbit (GEO)

Although there is no atomic oxygen at GEO (35,900 Km Altitude), the other hazards remain, and the problem of particulate radiation becomes more severe. The orbit passes through one of the van Allen radiation belts where there are many trapped electrons and protons. These ionizing particles damage materials by virtue of high local energy transfer, which causes chain scission in polymers.

Surface charging is another effect thought to be important in this orbit (Reference 5). In GEO one can expect to build up potentials of hundreds or thousands of volts on exposed surfaces. The record is 2200 volts in the sun. For surfaces in eclipse (LEO), the record measured potential is -19,000 volts. These surfaces must be conductive and electrically connected in order to spread such charges and prevent destructive discharging.

It is not definite that this is a significant problem. In the event that it is, one could possibly use canopy materials or inflatants that possess minimal conductivity to discharge the film, yet not enough to affect the measurements. There appear to be conductive polymers available that could be used in an outer layer of a canopy film laminate. In an article in the April 14, 1990 issue of Science News (p.230, by R. Weiss), the current status of polyaniline is discussed: Arthur Epstein of Ohio State University reported in the March 28 Journal of the American Chemical Society that his group has produced a processible polyaniline by a chemical doping reaction with sulfonate groups. Paul Smith of UC Santa Barbara has made polyaniline conductive by diffusive doping with chloride ions. Hexcel Corporation of Dublin, California announced on February 28 that it will begin the first large-scale production of polyaniline. It is not certain that polyanilines will have the other properties needed in an outer canopy layer; however, work on other conductive polymers is proceeding. Dupont is working on a conductive version of Tedlar®, for example.

Recommended Materials

The hazards described above limit the usable materials. In LEO organic materials will be quickly degraded unless protected by an impermeable skin. Only a fully oxidized surface or a noble metal surface can be used for a long term application if the surface properties must be retained for more than a few hours.

Unfortunately solid oxide surfaces are not ductile and foldable. A possible solution to this is to create a flexible silicone polymer surface for a plastic film which is then coated with vapor deposited aluminum. The aluminum will have a protective oxide natural coating. This will be exposed to atomic oxygen at the cracks that will occur due to folding; however, the oxygen will react with the silicone to make silicon dioxide that will resist further deterioration, and protect the structural polymer beneath. Although the silicon oxide is brittle, there should no longer be a need for flexibility after inflation. It is believed that this has not been tested under LEO conditions. It would not be suitable for GEO where the imperfectly conducting aluminum would build up charge in isolated regions.

In GEO, the best choice for a reflector surface would probably be vapor deposited gold. A very thin substrate film is recommended since it best protects a surface coating from the stress of folding. L'Garde experiments showed that gold coated surfaces retained almost all of their prefolded electrical conductivity. Cracks and pinholes may occur but such should not create a problem.

2.2.3 Testing

The most common thin films used in space inflatables are Mylar® and Kapton®. L'Garde has also used Tedlar® for its optical properties. There are, however, many more existing thin films that have never been tested or evaluated for the space environment. As part of this program, L'Garde searched for other films and ran simple tests to determine if any would have the advantage over Kapton® of requiring less pressure to pull wrinkles out of the film. The baseline system operates at a high pressure solely for this purpose, and therefore the weight of the replacement gas is relatively high. (Earlier tests indicated that a stress of 4.5MPa is needed to eliminate the packaging wrinkles from the three films mentioned above.)

Test Methods

Tensile testing was performed to determine the elastic modulus of the film. Tensile specimens, 25mm wide by 152m long, were pulled in a Tensometer (Model 10 -Monsanto) at a rate of 0.85 mm/s. The extensiometer was set at 51mm to eliminate the effect of specimen slippage on initial length. Four specimens per material were tested, half in the longitudinal direction and the remainder in the transverse direction. Elastic moduli were calculated for both directions from the data. These and manufacturer's values are shown in Table 2 along with brief identifications of the materials.

TABLE 2. THIN FILMS TESTED

Film Type[1] (& Composition)	Manufacturer	Thickness (Microns)	Elastic Modulus (GPa) Manufacturer		L'Garde	Available Thickness Range (Mils)
Dartek®, Type T420 (Uniaxial oriented polyamide, Nylon 66)	duPont Mississauga, Ontario, Canada	15	MD TD	2.93 2.59	3.46 2.48	0.6 - 1.5
Dartek®, Type 100-C101 (Non-oriented nylon 66)	" "	25	MD TD	0.69 0.69	0.68 0.58	15 - 100
Tuftane®, Type TF-330 (Polyurethane based on aromatic polyesters)	Lord Corp. Erie, PA	48	100% 300%	0.008 0.021	(2)	25 - 1500
MOPA/LDPE, (Nylon-LDPE Laminate-metalized) & OPA/LDPE, (Nylon-LDPE) Laminate	Metal Voto Greedmoor, NC	28	MD TD	-	2.21 1.06	-
HDPE, Type 950	Deerfield Plastic Inc.,S.Deerfield, MA	10		0.50 (3)	1.73	10 and up
HDPE/LDPE, Type 3303 (Blend of HDPE and LDPE)	"	28		-	0.37	-
NORMAT®, Type NMT (Aluminized) (Biaxially oriented Polypropylene, BOPP	Quantum Performance Films, Steamwood, IL	15	MD TD		5.89 3.68	-
Oriented Polypropylene propylene	Courtaulds Perfor Films Canoga Park, CA	30	MD TD	-	4.79 3.07	-
ATTANE®, Blend of polyethylene and poly(ethylene-Co-octene)	Bemis Co., Inc. Terre Haute, IN	46	MD TD	-	0.45 0.28	-
Valeron®, Type VLCP-2.5, (laminate of oriented PE-PE)	Vanleer Flexible, Inc. Houston,	63	MD TD	-	1.61 1.61	62 - 125
Mylar®, polyester	duPont	6.4	MD TD	3.63 3.78	4.08 4.32	6 - Up
Mellinex®, polyester	ICI Wilmington, DE	18		-	-	

---

1) Trademarks are those of the manufacturers listed.
HDPE: High Density Polyethylene, PE: polyethylene, LDPE: Low Density polyethylene, OPA MOPA
2) Accurate reading could not be obtained.
3) Reported in literature.

Simple cylindrical inflatables were made from each of the materials. Each was about 70mm in diameter by 280mm long. A valve was installed for pressurization. Half of the length of each cylinder was crumpled to simulate the creases and folds that an inflatable experiences during construction and packaging. It was then inflated with nitrogen. As the pressure was increased in increments, the smoothness of the surface was evaluated a) visually and b) by touch. The pressures at which the two surfaces (crumpled and "virgin") looked or felt alike were measured and recorded. (These pressures are insufficient to permanently remove wrinkles; that is, pressure has to be maintained.) Hoop stress was calculated: (pressure)(radius)/thickness.

Photographs were taken of each cylinder during testing. Figure 3 shows examples.

Observations

In examining the data (Table 3), it appears that elastic modulus, thickness and orientation of the film affect the stresses required to remove packaging wrinkles.

In general, required stress increases with both modulus and thickness. This was anticipated. If a material has a high modulus and/or is thick, it is more likely to be stressed beyond its elastic limit when folded. This creates a permanent crease which can be permanently removed only by yielding the film in tension. (This is a possible approach for inflated parabolic reflectors if the reflector's local radii of curvature do not change much, but is not being proposed in the baseline design.)

Orientation is very important. The non-oriented nylon film, Dartek® 100-C101, required about 40% more stress to achieve a relatively smooth surface than the oriented nylon, Dartek® T-420. Films that are not oriented (even those with a low initial modulus) suffer permanent deformations at folds. The material possibly becomes oriented at the folds, making them harder to remove, even temporarily.

There has been insufficient testing or analysis of these films for other required properties to make any recommendation. For instance, Tuftane® required minimal stress to remove packaging wrinkles. However, its modulus is so low that a paraboloid might stretch out of shape during manufacture, packaging and erection. Nylon-based films are more promising because of these tests. Nylon has other advantages (from prior work). It is more pinhole resistant and can take far more frequent folding and packaging than the popular space inflatable films. Versions of polyethylene-Nylon laminates also provide a good alternative method for bonding by melting the polyethylene to polyethylene.

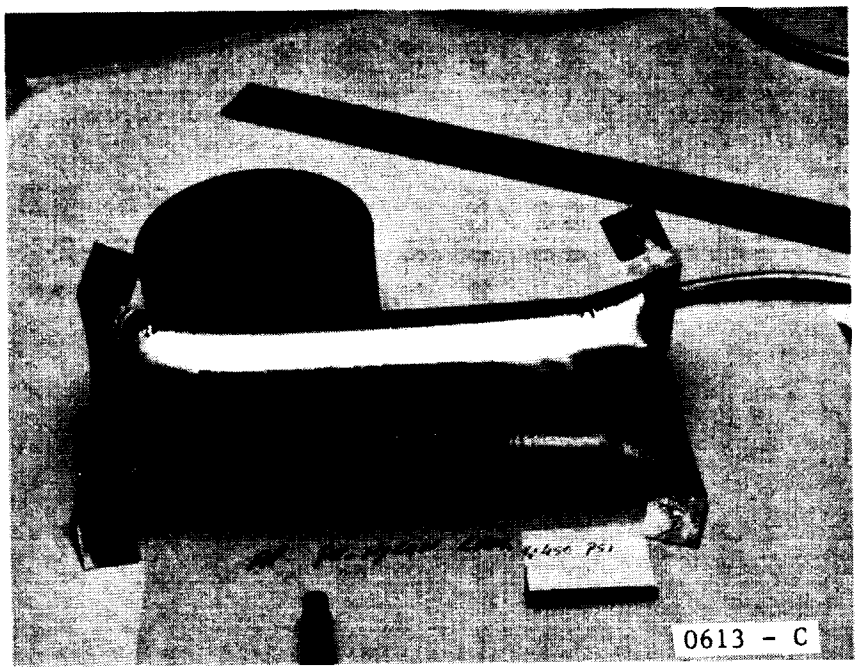

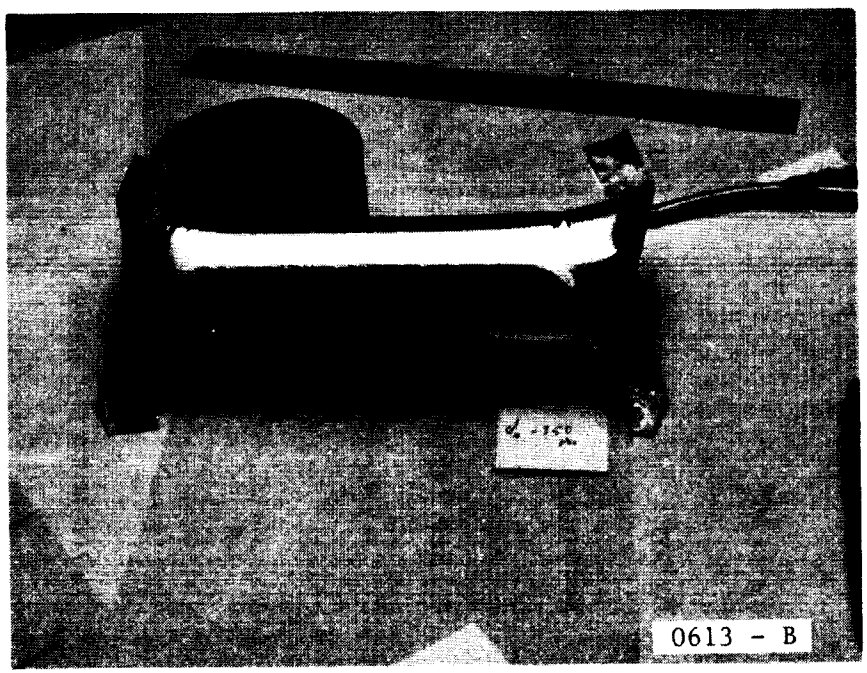

a) @ 1143Pa before the wrinkles are fully removed.
b) @ 2000Pa after visual removal of packaging wrinkles.
c) @ 2482Pa after finger-tip touch removal of packaging wrinkles.

(σ_H in photographs refer to hoop stress in the film.)

Figure 3. Cylinder made from Aluminized Nylon-Polyethylene Laminate (MOPA/LDPE Film

TABLE 3. STRESSES TO REMOVE PACKAGING WRINKLES

Film*	Pressure (Pa) Sight	Pressure (Pa) Touch	Hoop Stress (MPa) Sight	Hoop Stress (MPa) Touch	Plastic Modulus (GPa)	Thickness (Microns)
Dartek® T-420	1379	2137	3.10	4.83	2.93 3.46 MD 2.59 2.48 TD	15
Dartek® 100-C101	4481	11376	6.14	15.86	0.68 0.69 MD 0.58 0.69 TD	25
Tuftane® TF330	483	483	0.35	0.35	0.008 0.021	48
MOPA/LDPE	2000	2482	2.41	3.10	2.21	28
OPA/LDPE	1724	2620	2.07	3.17	1.06	28
HDPE, Type 950	690	690	2.07	2.07	0.50 1.73	10
HDPE/LDPE, Type 3303	1724	1724	2.07	2.28	0.37	28
Normat® BOPP	1793	2413	3.79	4.96	5.89 MD 3.68 TD	15
OPP	3654	5171	4.14	5.83	4.79 MD 3.07 TD	30
Attane®	2000	3034	1.52	2.28	0.45 MD 0.28 TD	46
Valeron®	10342	17237	5.38	8.96	1.61 MD 1.61 TD	63
Mylar®	690	827	3.45	4.14	3.63 4.08 MD 3.78 4.32 TD	6.4
Mellinex®	2275	2620	4.28	4.96		18

* See Table 2 for material identification and trademarks.

2.3 INFLATED PARABOLOID ACCURACY

The inflatable antenna is not a new idea but it is an idea whose time has come. Such systems were conceived, studied, built, and tested years ago, and the technology has evolved to make the ESGP concept practical. Sundstrand built a three-meter diameter and then a 14-meter diameter inflatable parabolic concentrator in the 1960 to 1964 period for use as a solar concentrator. Their system was rigidized after inflation in response to the great concern at the time about a meteoroid hazard which was largely unknown. Still, accuracies were sufficient to show that such a system could work as a concentrator for a solar power system. Sheldahl built an inflatable three-meter diameter microwave antenna that was tested at 2, 3 and 4 GHz in 1965. This was also quite successful, and accuracies of about 3mm RMS were demonstrated on the ground. Suppression of side lobes was directly measured, and varied from -15.0 to -21.5db. Even without optimization of the feed design feasibility was clearly demonstrated.

More recently, L'Garde has been developing inflated collectors. The next subsection describes part of this work in which accuracies of 1 mm RMS has been achieved. Subsection 2.3.2 relates such accuracy results to gain and resolution.

2.3.1 L'Garde Programs

The purpose of the Highly Accuracy Inflatable Reflector (HAIR) I Program (Reference 7) was to investigate methods of joining flat gores and to identify sources of error that, when eliminated, would lead to surface accuracies on the order of 0.1mm. It was determined that minimal errors resulted when the gores were joined by bonding with 10mm wide tape of the same material and thickness as the gores. Tests conducted showed that the effect on surface accuracy of the seams could be reduced to errors on the order of 0.1mm RMS. Figure 4 shows the results of surface measurements of two membranes. The standard is a 25 micron thick flat sheet with no gores or seams. The other is a membrane constructed of 25 micron thick gores joined with 25 micron thick tape. The difference between the two curves represents an RMS surface error of 0.13mm.

During the HAIR II Program (Reference 8), the reflector was developed for a solar rocket application which requires two off-axis reflectors each 30m in diameter. The 1m on-axis work was scaled up to a 3m system. One of the test membranes is shown in Figure 5. This reflector (f/D = 1) was completely mapped and had an overall surface accuracy of 1.15mm RMS.

In an early attempt to determine how to accurately build inflatable antennas, L'Garde developed the FLATE code. FLATE solves the equations for small deformations of a parabolic structure to determine precisely the shape of the flat patterns used to manufacture a paraboloid. FLATE could handle seams only approximately. A better design tool was sought and developed under a classified program aimed at inflatables technology improvement. Attempts to use existing finite element codes to analyze inflatable structures have proved fruitless because the shell bending theory used by these codes is not applicable to the case of a shell membrane with large deflections and small strains. A new analytic tool was required, and has recently been completed--LDIPS.

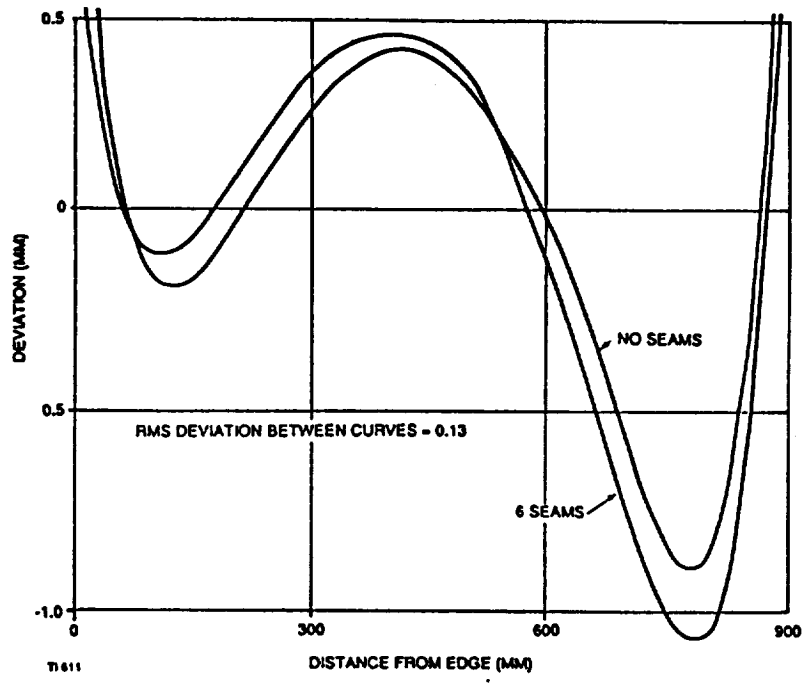

Figure 4. Surface Error Due to Seams

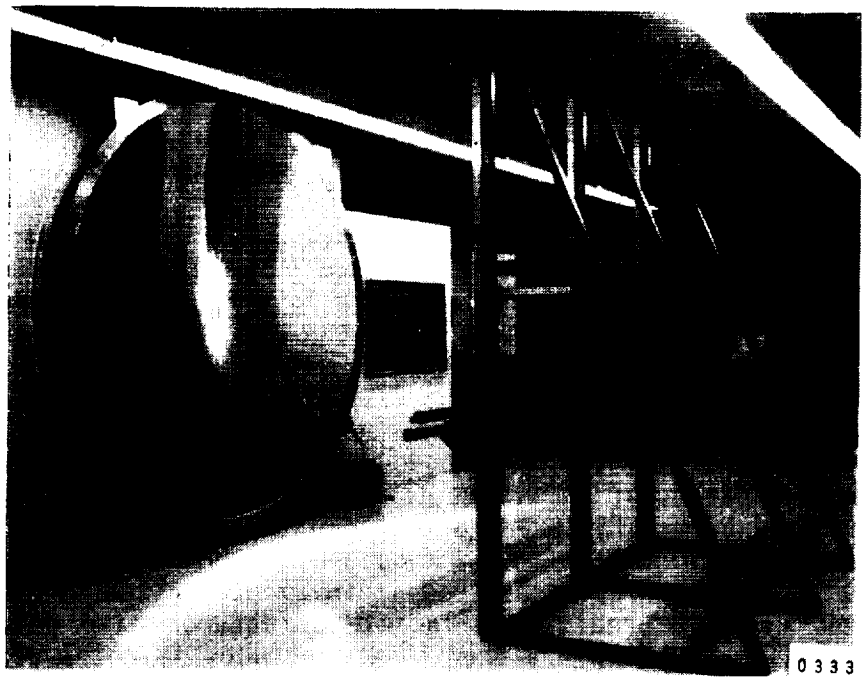

Figure 5. 3m Test Reflector

The total inflation process can be modeled by solving for the equilibrium state of the membrane at successively higher pressures. Figure 6 (dimensionless coordinates) shows LDIPS results for a high-pressure case. As the pressure is increased, LDIPS shows the change in profile approaching the "exact" case. The deviation between the LDIPS final result and the "exact" paraboloid is due to the fact that the linear theory used by FLATE was not sufficiently accurate to produce the proper starting profile. When FLATE was corrected to use the same large-deflection model for stress-strain as LDIPS, they produced the same result as shown in Figure 7 for cases of three different Poisson ratios.

Besides the paraboloid, the design and construction of the supporting torus at the outer edge of the paraboloid is critical. The problem is complicated by the fact that the off-axis paraboloid must be supported by an elliptical structure. L'Garde has studied the problem of the torus design for years and has recently solved the problem as part of the Deployable Solar Concentrator Experiment (DSCE) Program. The result was the computer program RIM (Reference 1)which calculates both loads and deformations in the torus supporting an off-axis paraboloid structure. The details of this analysis have been accepted for publication in a two-part paper in the Journal of Aerospace Engineering (ASCE).

The existence of these sophisticated codes to aid the design of precision inflatable structures makes the ESGP concept practical. These tools although developed on other programs, directly support the antenna design.

2.3.2 Gain and Resolution of Parabolic Antennas

For a perfectly shaped parabolic reflector (circular aperture), the gain can be expressed in terms of the area and wavelength as

$$G = \eta \cdot \frac{(4\pi)\ (\pi D^2/4)}{\lambda^2}\ , \qquad (1)$$

where G = Gain
D = Aperture diameter (reflector small diameter)
λ = wavelength
η = 0.65 = Aperature efficiency based on 10dB edge illumination taper.

The relationship between the gain and the beam width can be expressed as

$$G = \frac{27{,}000}{\alpha \cdot \beta}$$

where α and β are the half power beamwidths (in degrees) of the radiated pattern in the electric and magnetic planes respectively. Here it will be assumed that $\alpha = \beta$.

Equation (1) can be modified to take into account surface imperfections. Statistically random mechanical deviations lead to the relationship

$$G = G_o\ (1 - \delta^2)$$

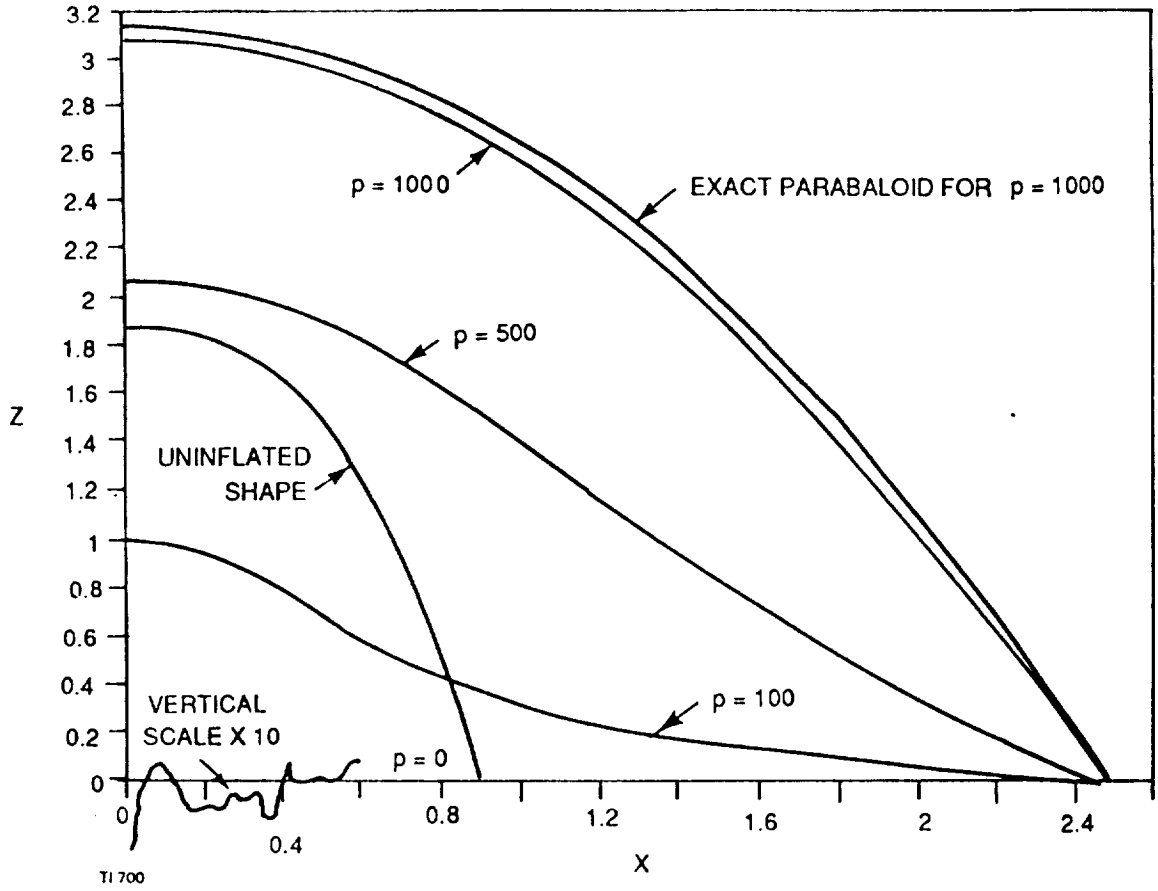

Figure 6. LDIPS Modeling of Inflating Paraboloid

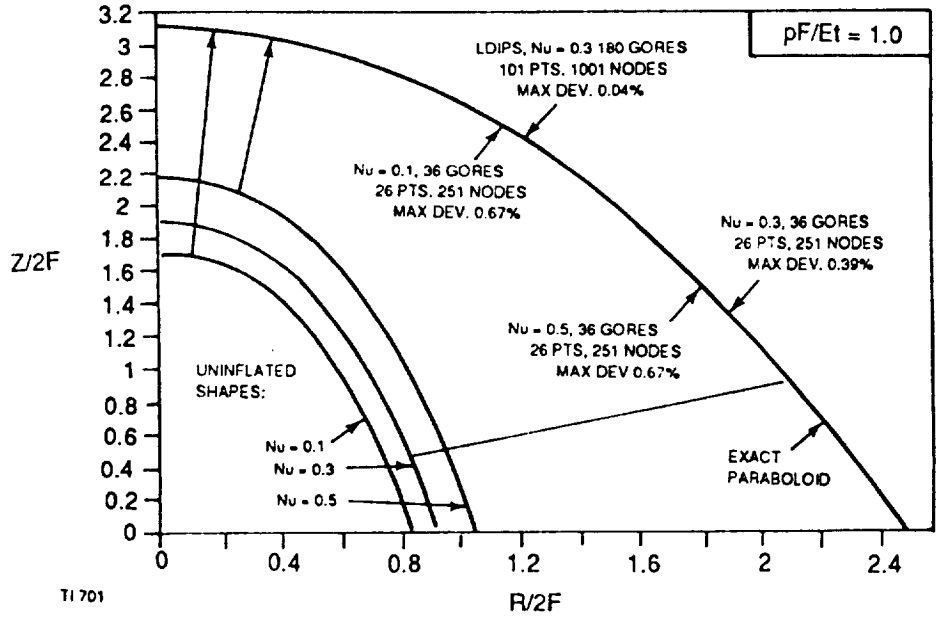

Figure 7. LDIPS Validation by Comparing to Exact Solution

where G_n = antenna gain with perfect reflector as given by equation (1)

δ = RMS surface tolerance in radians

It is assumed here that the surface errors are small compared to the wave length ($\delta \leq \lambda/28$). The surface tolerance in radians can be found from

$$\delta = \frac{4\pi t}{\lambda},$$

where t is the RMS surface error given in the same units as λ.

Assuming that resolution is defined as it is for a conventional closed loop tracking radar, then targets 0.85 times the beamwidth may be resolved.

Explicitly,

$$\text{Resolution} = 0.85 \times 2R \tan(\alpha/2),$$

where R = Distance from antenna to target,
α = Antenna half power beamwidth.

Using these equations, a graph has been generated to illustrate the relationship between gain vs. reflector diameter and frequency (Figure 8). A surface inaccuracy of 1mm RMS was used as a reasonable estimate of what can be achieved with an inflatable reflector. A graph (Figure 9) has also been generated to show the resolution of an inflatable reflector in the range of 12 to 40 meters in diameter at frequencies between 6 and 10 GHz. The same 1mm RMS accuracy was used and an orbit of 1000 km was assumed. The resolution scales linearly with the orbital attitude.

From the graphs it can be seen that both resolution and gain improve at higher frequencies. It should be pointed out, however, that the model used assumes that the wavelength is large compared to the RMS surface errors ($t \leq \lambda/28$). Because of this, the data presented cannot be extrapolated to frequencies greater than 10 GHz. The graphs also show that both resolution and gain improve with increases in reflector diameter. This relationship depends in part on the assumption that reflector RMS surface accuracy is independent of the reflector size. Experience shows that this assumption is reasonable.

Some of the accuracy data gathered as part of the HAIR Program (Figure 10) was given to Dr. Warren Stutzman of the Virginia Polytechnic Institute for evaluation. They determined that the RMS surface error was 2mm RMS for the data given them. Their Reflector Antenna Program (RAP) is a physical optics routine developed at Virginia Tech to calculate the loss in gain due to the surface inaccuracies (Reference 9). It was found that the gain losses are 0.4dB and 1.36dB at 2.82GHz and 7.07GHz, respectively, for the HAIR antenna. Calculated radiation patterns from their report are shown in Figures 11 and 12. The inflated reflector works in the low (~ 10) GHz range.

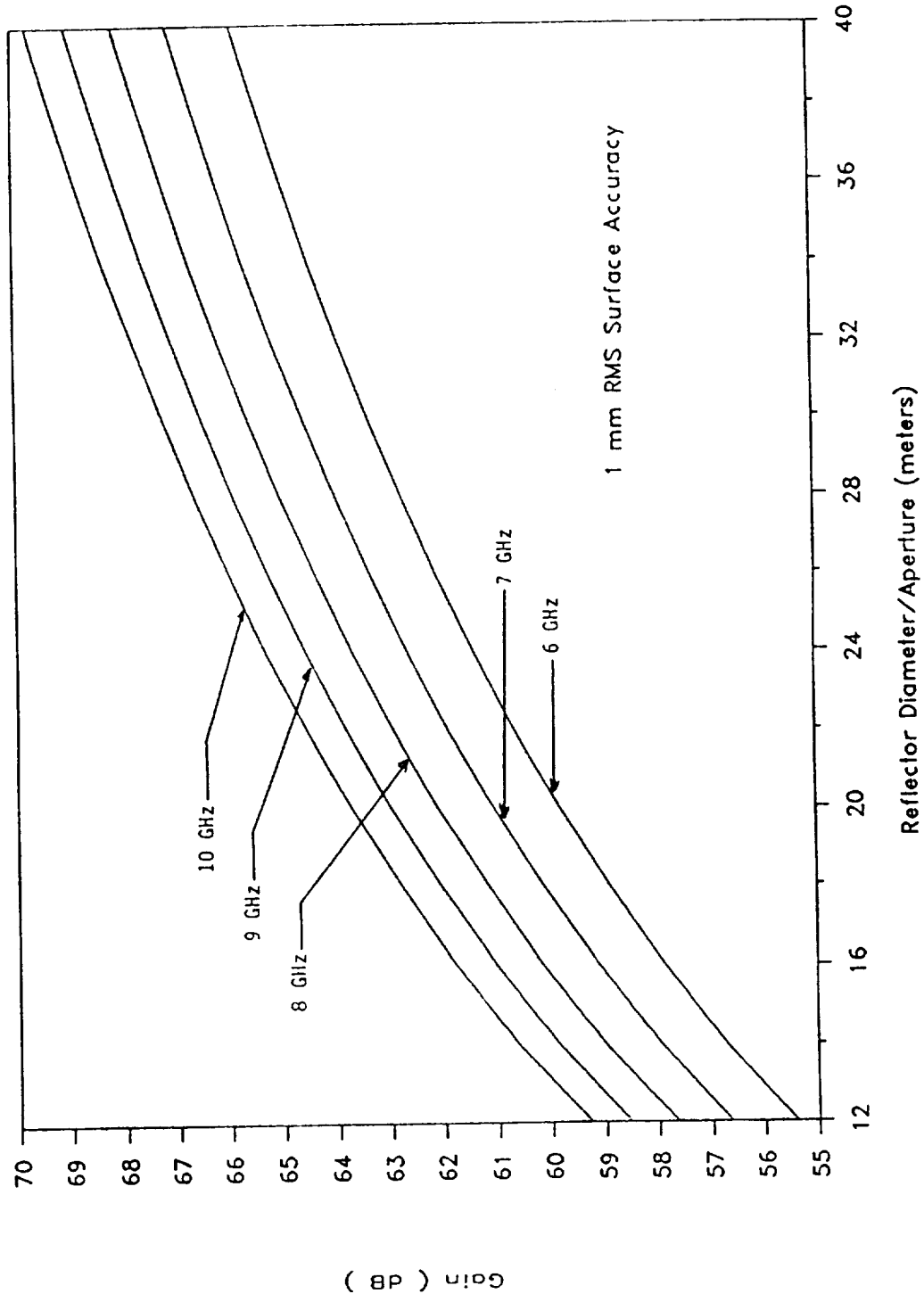

Figure 8. Gain vs. Reflector Diameter at Various Frequencies

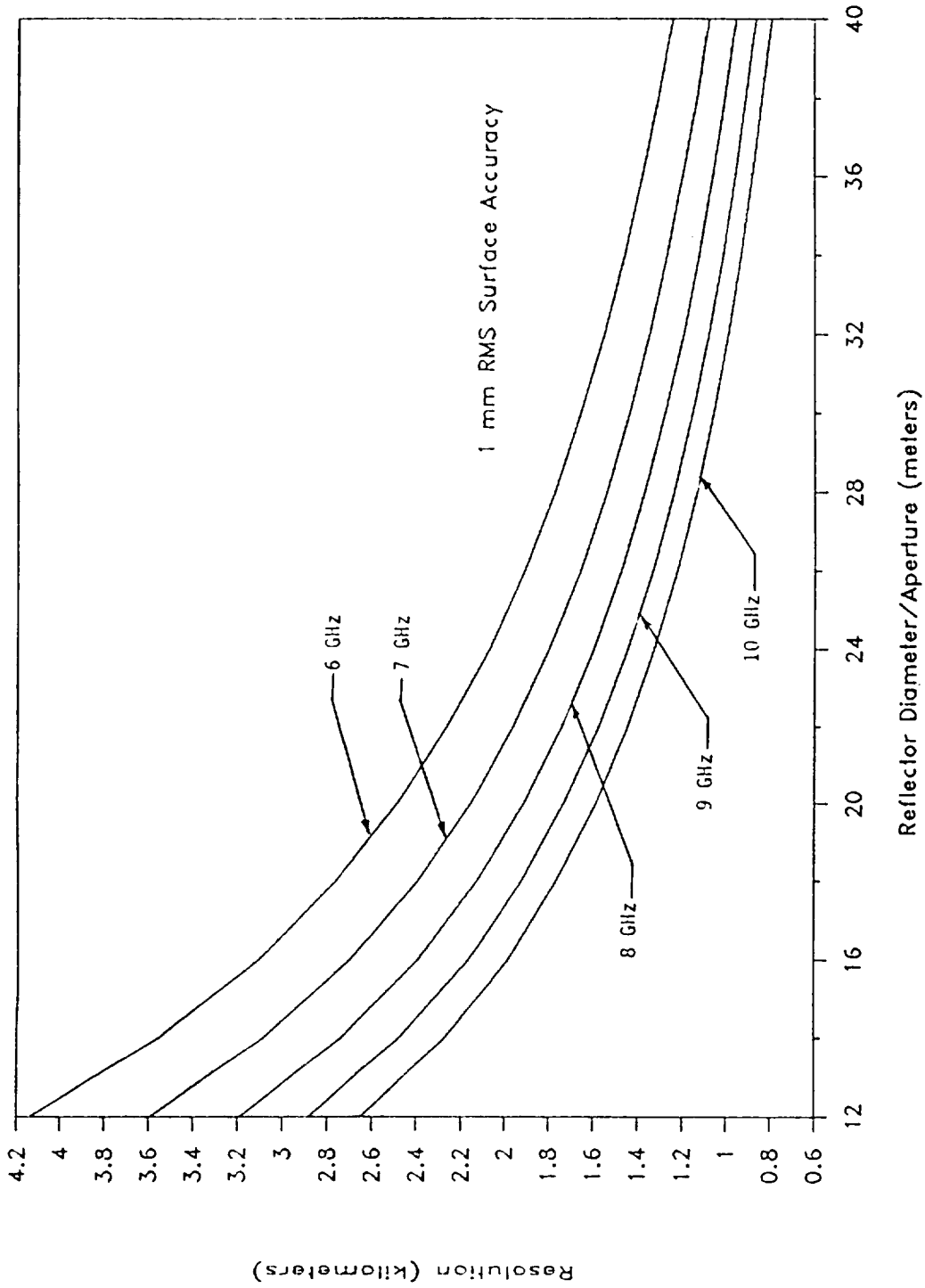

Figure 9. Resolution vs. Reflector Diameter at Various Frequencies

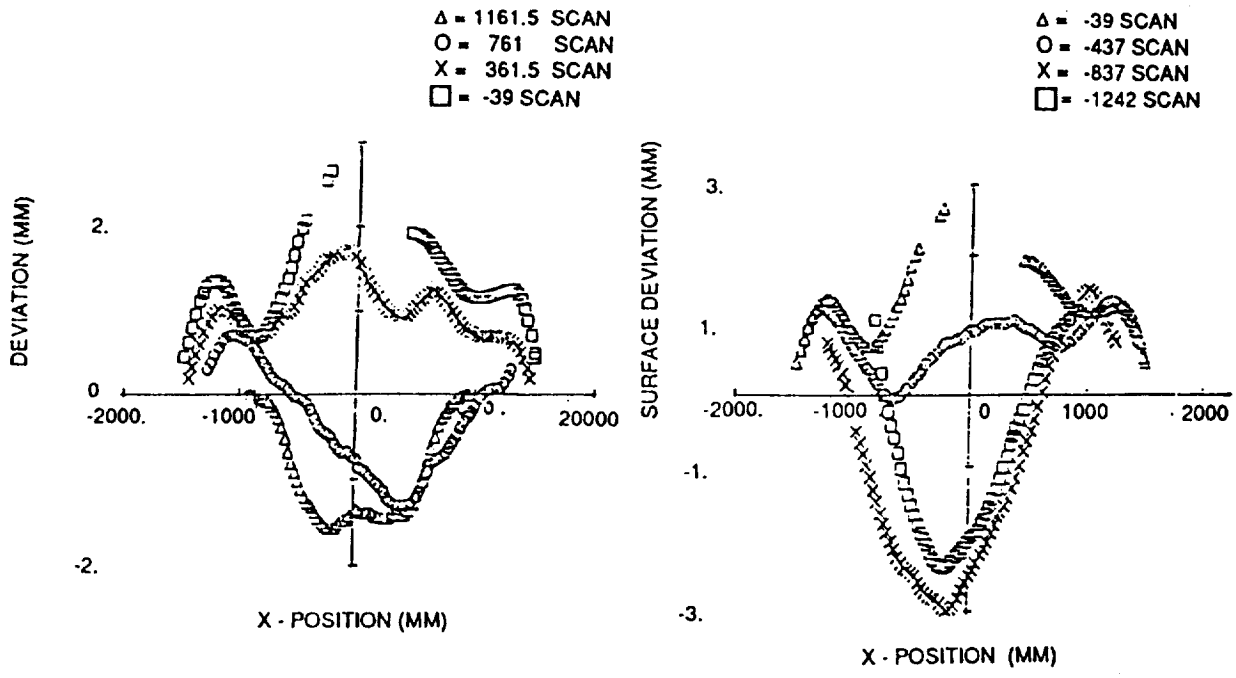

Figure 10. Plot of Surface Error

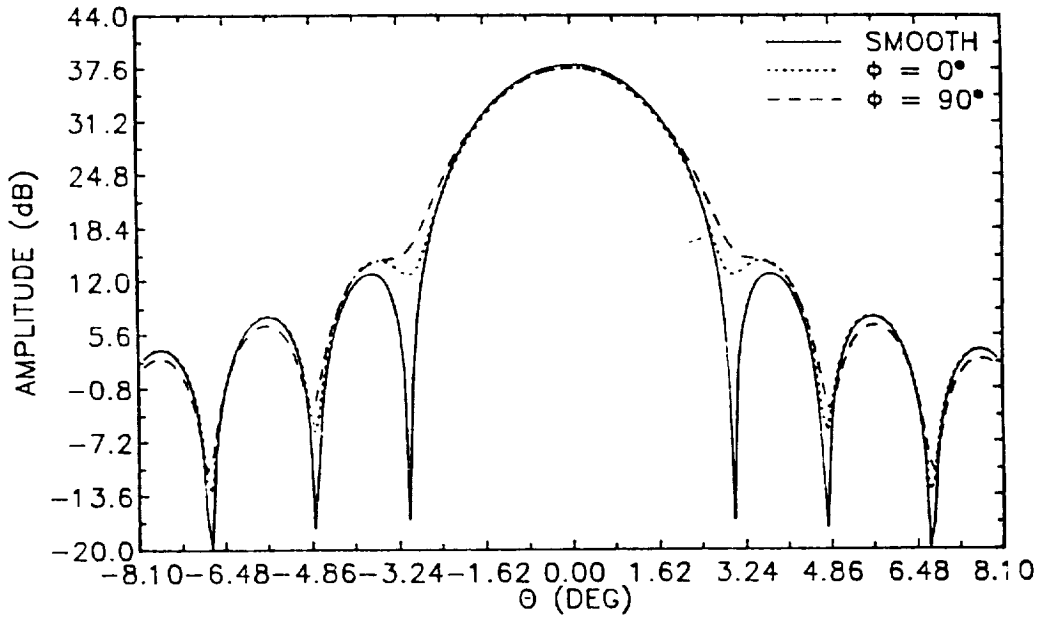

Figure 11. Radiation Patterns Calculated for the HAIR Reflector at 2.82GHz using RAP

The ESGP concept is to work at frequencies lower than 6 GHz to as high as 60GHz without side lobes. Based upon the above analyses and previous tests, L'Garde believes inflatables will never meet ESGP requirements at frequencies approaching 60GHz. However, at these high frequencies only a small antenna is needed. Therefore, the ESGP concept contains a rigid, 4.2m diameter reflector for the high frequency requirement. The inflatable will provide this rigid reflector with a better thermal environment than what it would have on its own. For frequencies up to about 10GHz, L'Garde has high confidence that inflatable reflectors will work for the ESGP, and this is the region where very large reflectors are needed.

2.4 THERMAL

The use of the inflatable antenna in conjunction with a smaller precision structure can provide the thermal stability needed for the enclosed precision structure at short wavelengths. Inflatables offer better thermal control opportunities than open structures. The radiative exchange between the sides of the inflatable can sharply reduce temperature non-uniformities. Special coatings on the Explorer IX balloon satellite reduced the maximum differential temperature across the balloon from 120°C to 30°C (Reference 10). Grid-like antennas have poor radiative exchange characteristics so a requirement for isothermality cannot be met; either materials of extremely low thermal expansion must be used, or the antenna shape must be actively controlled. Hughes has covered an antenna with a Kapton® film solely to protect the antenna dish from temperature changes (Reference 11). The ability of these continuous area elements making up a balloon to control temperature caused NASA to seriously consider encapsulation of satellites in balloons as a method of thermal control (Reference 12). This characteristic of the inflatable antenna makes the hybrid system extra attractive.

L'Garde took a preliminary look at the thermal aspects of the ESGP design, and was encouraged. However, more extensive modeling is necessary. The ESGP thermal design is incomplete. It is probable, however, that it will be done without resulting in a significant weight penalty.

PANT is an existing thermal analyzer code designed and optimized for the paraboloid-cone geometry and the thin film antenna at steady-state. Figure 13 shows the general paraboloid-cone antenna and the coordinate system used to describe it. (Reference 13) PANT calculates the radiative heat exchange among the surfaces making up the paraboloid-cone system. It also includes a ray tracing feature which calculates the net energy received by surface elements as a result of non-zero material solar transmissivities. This feature may be turned off by inputting zero transmissivity values.

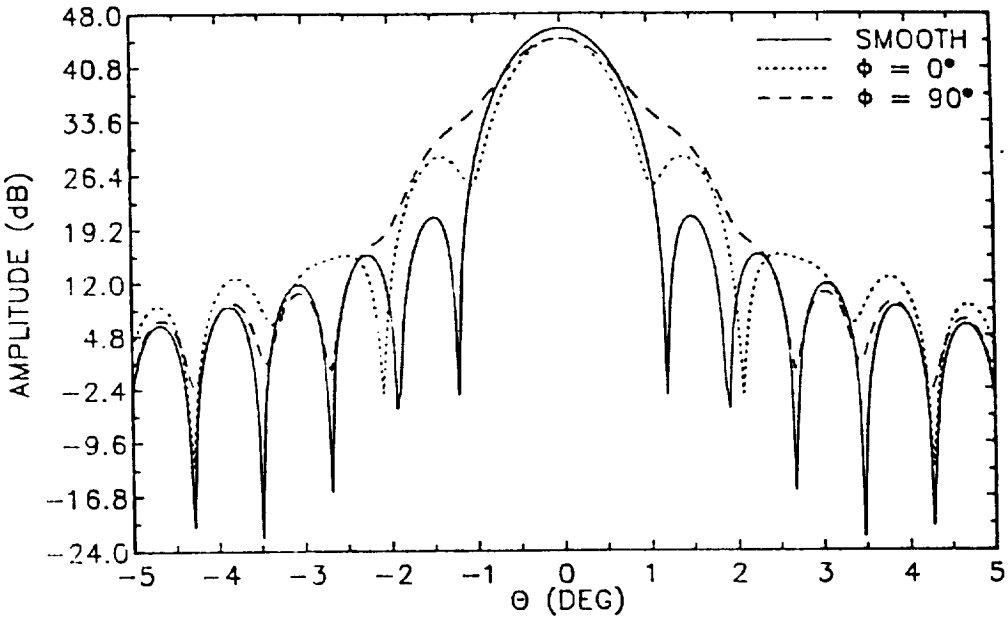

Figure 12. Radiation Patterns Calculated for the HAIR Reflector at 7.07 GHz using RAP

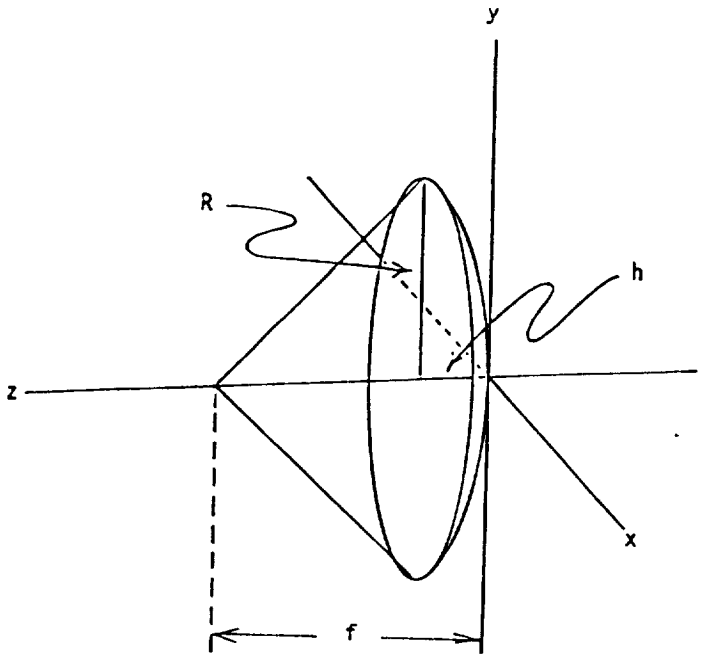

Figure 13. Generalized Antenna and its Coordinate System

The surface area of the system in Figure 13 is automatically discretized into a number of elements much like in a finite element or finite difference analysis. The radiant energy exchange between these elements are then calculated and the temperatures of each of the elements is saved. The input to PANT consists of

- antenna diameter
- F-number
- desired number of elements into which the antenna is to be discretized.
- angle between sun and antenna axis
- external emissivity of paraboloid
- internal emissivity of paraboloid
- external reflectivity of paraboloid
- internal reflectivity of paraboloid
- solar transmissivity of paraboloid
- external emissivity of cone
- internal emissivity of cone
- external reflectivity of cone
- internal reflectivity of cone
- solar transmissivity of cone
- number of Monte Carlo rays traced
- seed for random number generator

In order to be able to use PANT to analyze the ESGP, the off-axis paraboloid was approximated by an on-axis reflector with approximately the same surface area. The on-axis model parameters have also been chosen so that the cone will have approximately the same surface area as the canopy. It was assumed that there were no meteoroid shields inside the inflatable. The PANT model for the ESGP 28m antenna was described by the following inputs.

Reflector:

Focal length:	35m
Diameter:	28m
Surface Area:	653.67m^2

Cone (canopy):

Focal Length:	35m
Radius:	14.35m
Surface Area:	1644m^2

For the thermal analysis by PANT, 100,000 Monte Carlo rays have been used. A total of 120 area elements was requested and PANT, constrained to make the area elements approximately equal, was able to come close - 110 elements total. This discretization is shown in Figure 14. The element numbers are indicated together with the element numbers on the opposite side which are enclosed in parentheses.

2.4.2 Results

Figure 15 shows the results using the above thermal model, and the properties of Kapton® film. Translucent Kapton® is used in the baseline ESPG design, with the reflector being metallized.

As can be seen, temperature changes significantly with solar aspect angle. We do not know what differential temperatures are acceptable, but certainly a constant temperature independent of solar aspect angle is preferred. The Figure 15 temperature range is ± 80K.

Figures 16 and 17 use opaque white or black film, respectively, rather than the translucent Kapton®. The temperature range for black Kapton® is ± 70K, and the temperature range for white is ± 50K. These two figures indicate that a black Kapton® balloon with white ink on the external reflector surface will decrease the spread. This was run and is shown in Figure 18. The maximum temperature range is 240K ± 32K, a significant improvement. (Black Kapton® is available in a 25 micron thickness, but not yet available in a 7.6 micron thickness. Applying black ink to regular translucent Kapton® is practical; however, such may not meet other requirements.)

The 32K temperature spread shown in Figure 18 is actually a gradient across the reflector when the sun is broadside to the antenna. Again, we do not know what is acceptable -- only that no gradient is preferred.

Approaches to reducing the gradient have not been explored because more extensive modeling for the true configuration is required. The model should include the hemispherical (rather than conical) canopy and the meteoroid shields. It is likely that the meteoroid shield that is in the plane of the elliptical torus can be used. This shield (perhaps of a different shape) will help keep solar energy from reaching the reflector for aspects less than 80°. A radiation shield external of the reflector may also be appropriate for larger solar aspect angles.

As noted earlier, thin films (which are low in weight) are extensively used for thermal control. It is expected that good thermal designs can be derived for the ESGP and flight experiment concepts.

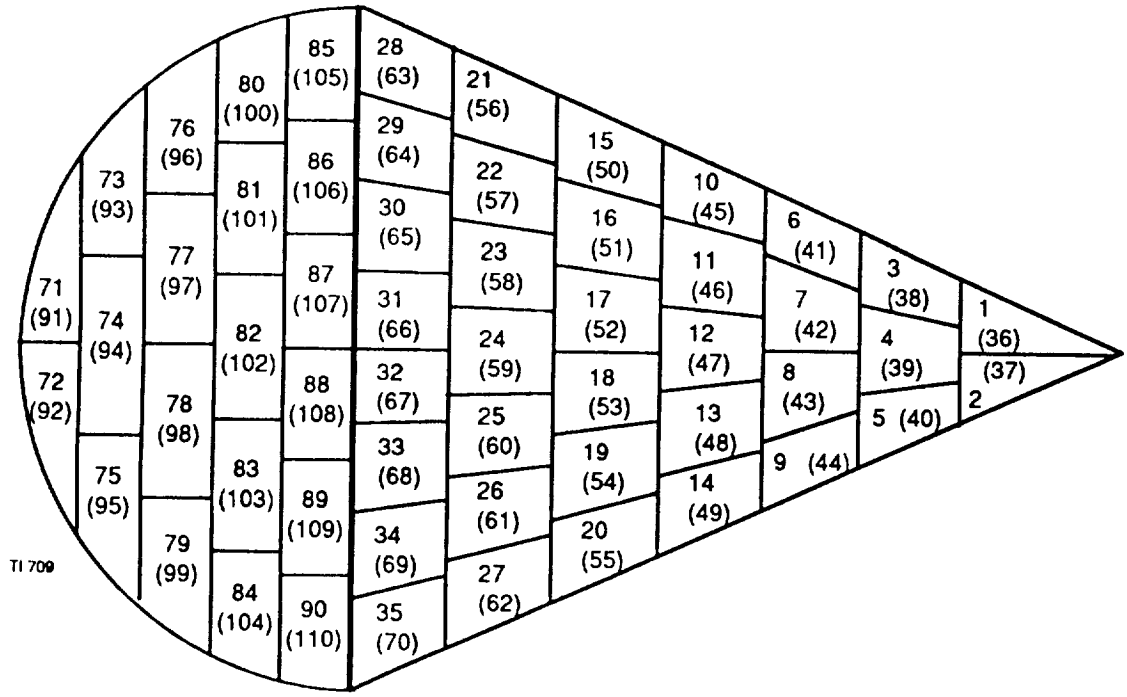

Figure 14. Model's Area Elements

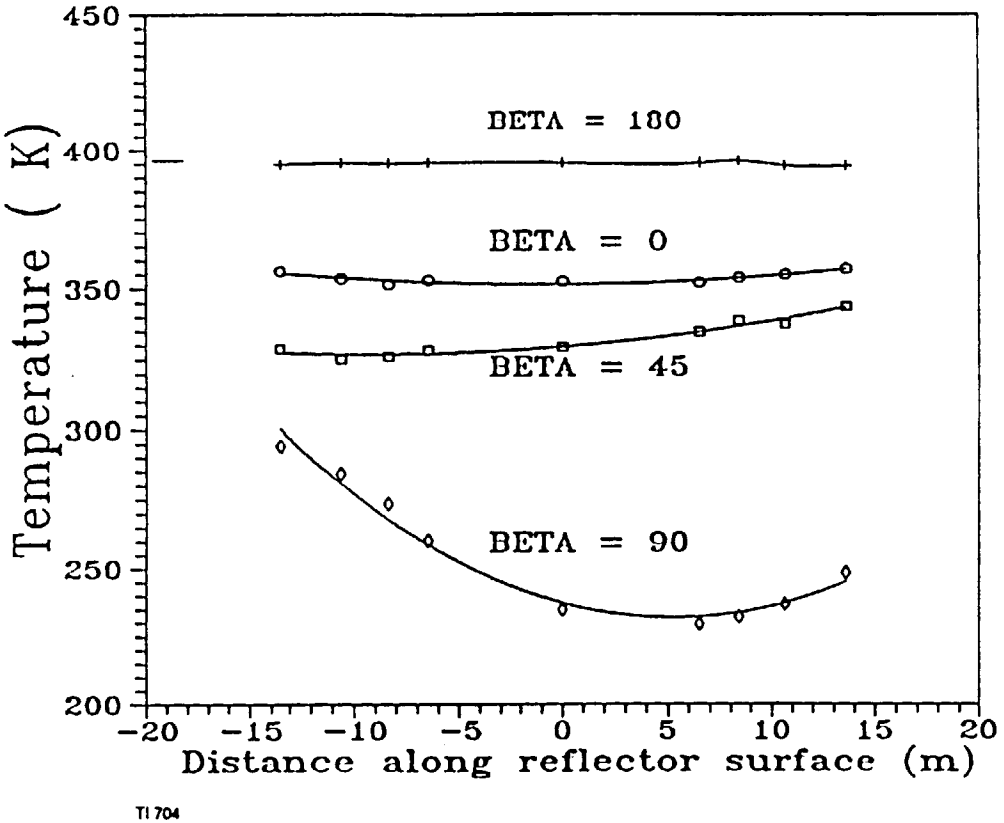

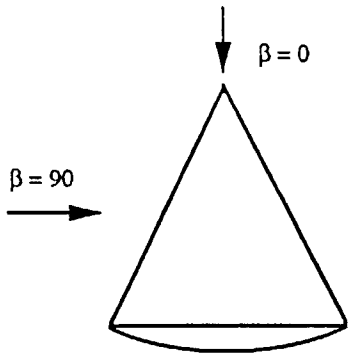

	REFLECTOR	CANOPY
EMISSIVITY		
EXTERNAL	0.05	0.88
INTERNAL	0.05	0.88
SOLAR		
ABSORPTIVITY	0.1	0.33
TRANSMISSIVITY	0.0	0.53
REFLECTIVITY	0.9	0.14

Figure 15. Kapton® Reflector Temperature

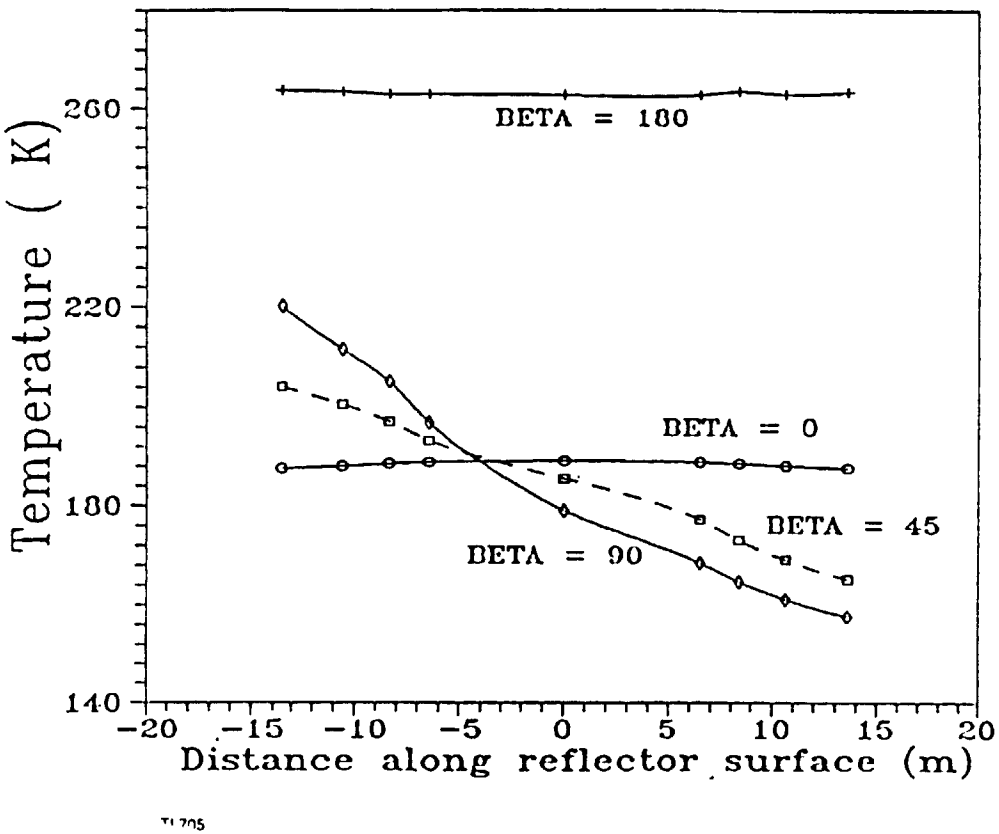

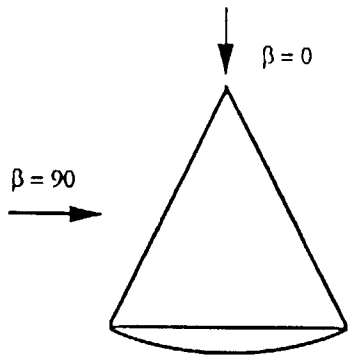

	REFLECTOR	CANOPY
EMISSIVITY		
EXTERNAL	0.9	0.9
INTERNAL	0.9	0.9
SOLAR		
ABSORPTIVITY	0.3	0.3
TRANSMISSIVITY	0.0	0.0
REFLECTIVITY	0.7	0.7

Figure 16. White Film Reflector Temperature

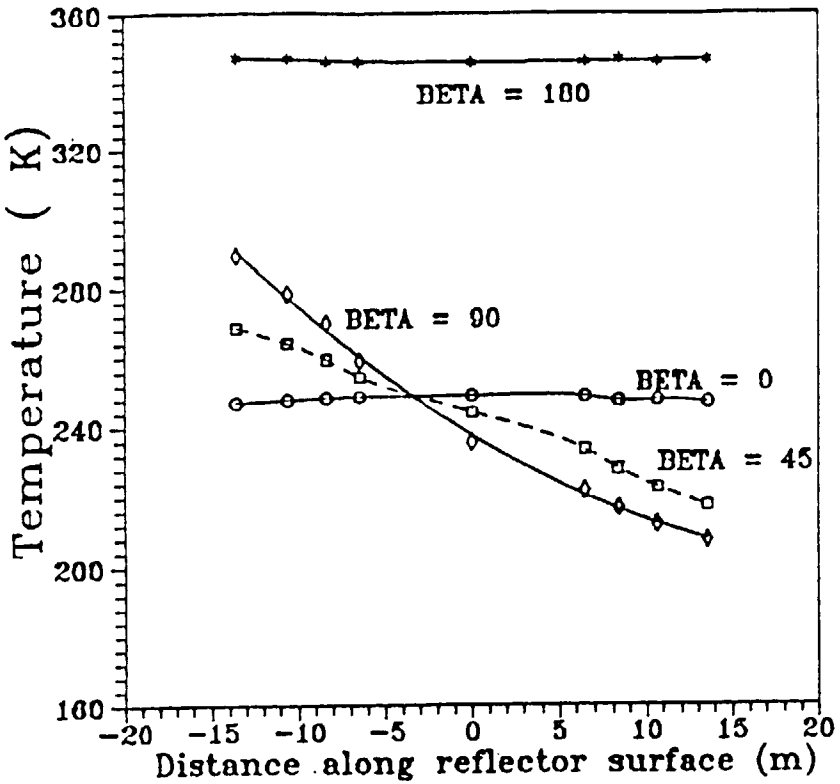

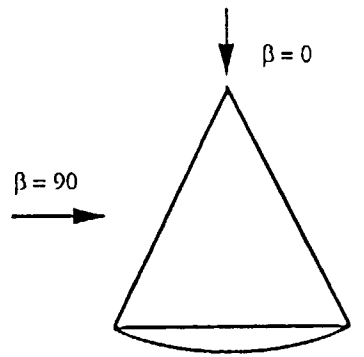

	REFLECTOR	CANOPY
EMISSIVITY		
EXTERNAL	0.9	0.9
INTERNAL	0.9	0.9
SOLAR		
ABSORPTIVITY	0.9	0.9
TRANSMISSIVITY	0.0	0.0
REFLECTIVITY	0.1	0.1

TI 706

Figure 17. Black Kapton® Reflector Temperature

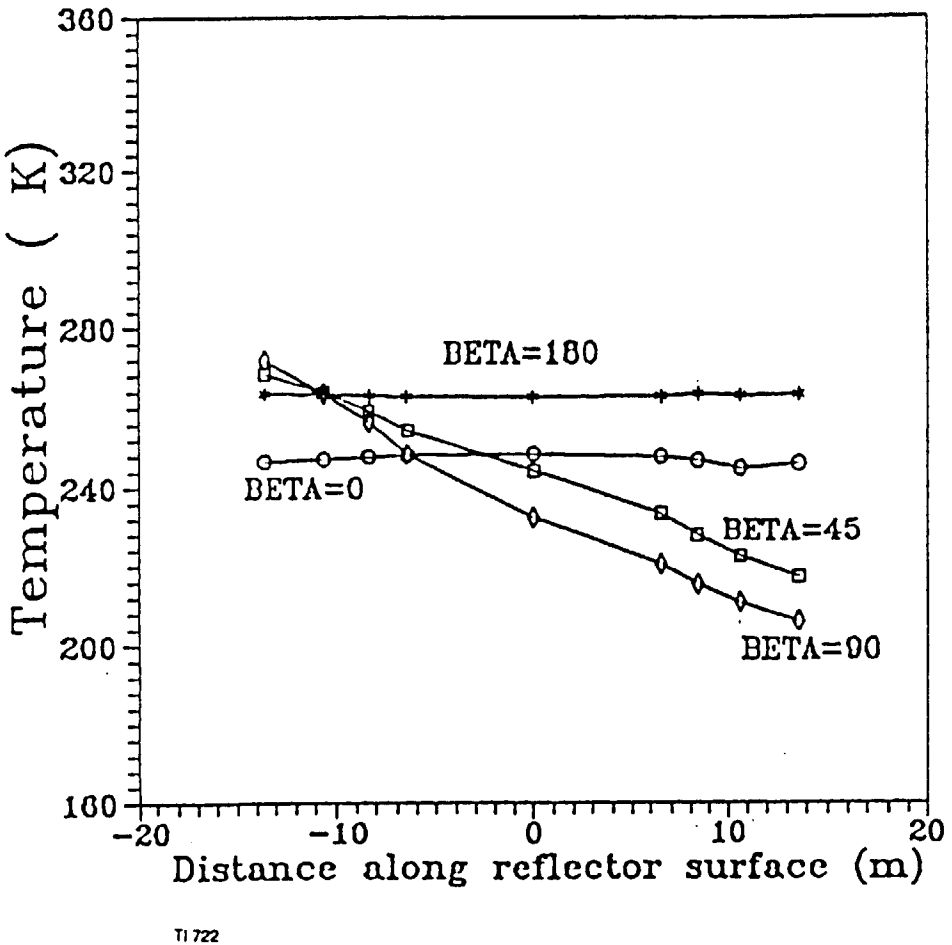

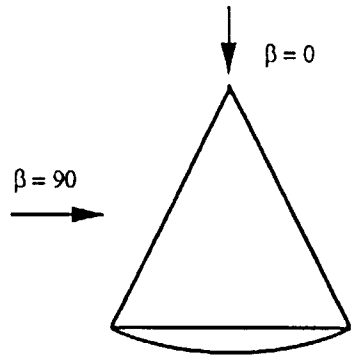

	REFLECTOR	CANOPY
EMISSIVITY		
EXTERNAL	0.9	0.9
INTERNAL	0.9	0.9
SOLAR		
ABSORPTIVITY	0.3	0.9
TRANSMISSIVITY	0.0	0.0
REFLECTIVITY	0.7	0.1

Figure 18. Reflector Temperature Spread Reduction Using Tailored Optical Properties

3.0 FLIGHT EXPERIMENT

There are three prime objectives for the flight of a large inflatable antenna, all of which require space flight for accomplishment.

1. Validate erection of a packaged 28m off-axis parabolic antenna.

2. Determine surface accuracy of the paraboloid as a function of internal pressure and sun aspect angle.

3. Determine the structural dynamics of a large inflatable.

Fulfilling Objective 2 inexpensively and reliably was the main aspect influencing the experiment design.

Initially, L'Garde planned to radiate the ground from LEO in a manner similar but inverse to the end use of ESGP. Inexpensive receivers/recorders would be laid in a long line normal to the orbit. As the flight units passed over the receivers, data would be recorded that could be translated into accuracy. However, 1) milliradian-type pointing accuracy was required, and 2) at most only two passes over the receivers were possible because of the ever changing orbital earth track and the short life of the experiment due to drag. This approach was abandoned because this was too little data at too high a risk. Other methods were explored. NASA/Langley used stereo optical techniques to measure the surface accuracy of their large electrostatically-formed paraboloid antenna in the early '80's. However, the use of precision optical components in space would likely raise the cost of this experiment. L'Garde used a laser ray-tracing method to map the surface accuracy for the 1m and 3m diameter inflatable antennas. However, the laser must be steered in some fashion to obtain the data--difficult in a flight experiment.

McDonnell Douglas developed a method of measuring surface accuracy based on a Digital Imaging Radiometer (DIR) which recorded by video the patterns of light reflected from the paraboloid from a series of individual lights. This system has been used to evaluate the slope error ("waviness") and radius of curvature of approximately 100 3 ft. x 4 ft. mirror modules and to align eight 25 KW dish concentrators, each having 82 mirror modules. This system has been operational for over 4 years, and has been completely verified by an extensive series of field tests of operational solar concentrators.

The DIR approach provides very large amounts of accurate slope data in a short period of time, is typically used in standard manufacturing buildings, requires no special control of temperature, air gusts, etc., and allows for substantial oscillatory movement of an entire dish concentrator, as would be caused by air currents.

The MDSSC DIR can be used to evaluate curved mirror modules of virtually any size. Evaluations have been made on modules from 1 ft. x 36 ft. The existing system has obtained the following data: 1) 75,000 to 100,000 data points of slope error at discrete points on reflective surface, accurate to ± 0.05 mrad 2) overall cant angles for mirror modules, sections of modules, or total concentrator, accurate to ± 0.1 mrad, 3) overall average slope error of modules, accurate to ± 0.1 Mrad, and 4) pointing error of modules or concentrator, accurate to ± 0.1 mrad.

The principle behind the DIR can be exploited for the flight test. If the reflector were a spherical segment instead of a paraboloid, a light were located at the radius of curvature of this surface, and the spherical segment viewed by a camera in this same vicinity, a perfect surface would result in a uniformly lit image. Portions of the surface that are in error would show up black (unlit) since the reflected light would be off course. If the single light is replaced by a bank of lights so that they are located close to but not at the center of curvature, then the surfaces in error will show lit up for some of the lights. By sequencing through a series of such lights and recording the images, the surface contour can be accurately reproduced. The number of lights needed is increased if the surface deviates much from a sphere or is grossly inaccurate. However, for the accuracies L'Garde has already demonstrated in the lab on inflatable reflectors and for the geometry shown below, a small bank of lights (about 1.3m diameter) is sufficient. Even for gross distortions in the reflector surface, high accuracy measurements will be possible for certain areas of the reflector, and high accuracy will not be needed for characterizing the gross distortions.

Therefore, the selected measurement device is a bank of lights and a TV camera located roughly at the center of curvature of the paraboloid. This selection greatly affected the hardware design. The center of the ESGP 28m antenna is offset from the vertex by 38 meters and its focal length is 56 meters. In order to be able to use the surface imager to obtain accuracy data, the flight experiment 28m antenna has a 14m offset and 28m focal length. This change greatly reduced the length of the inflated structure and the diameter of the erected light panel for the surface imager. However, the baseline is still an off-axis 28m paraboloid, and the resulting data will be directly applicable.

The ESGP concept has a torus and struts that self-rigidize after inflation, while this proposed baseline does not. The extra cost to complete development of the self-rigidizing structure did not appear warranted for the experiment because this short LEO flight will not contribute significantly to the structure's development. The self-rigidizing structure can be developed on the ground, and would eventually have to be validated above LEO orbits.

3.1 HARDWARE DESCRIPTION

The packaged system will weigh as much as 200 kg and occupy about 0.4 cubic meter of volume. About half of the volume is a packaged inflatable, so the package shape can be easily adapted to the space available on the launch vehicle. The desired shape is a pancake as large as 1.25 meters in diameter. Figure 19 shows the hardware after deployment and inflation.

3.1.1 Ejector

Ejector detailed characteristics are greatly dependent on launch vehicle constraints. For enhanced safety and low weight, the ejection velocity will be as slow as practical, perhaps as low as 0.1 m/s. The energy required, roughly 1J, will be provided by springs. Pyrotechnics will be used to initiate ejection.

Ejection accuracy (tolerances, tip-off) requirements will be derived from launch vehicle safety requirements -- not by any experiment objectives.

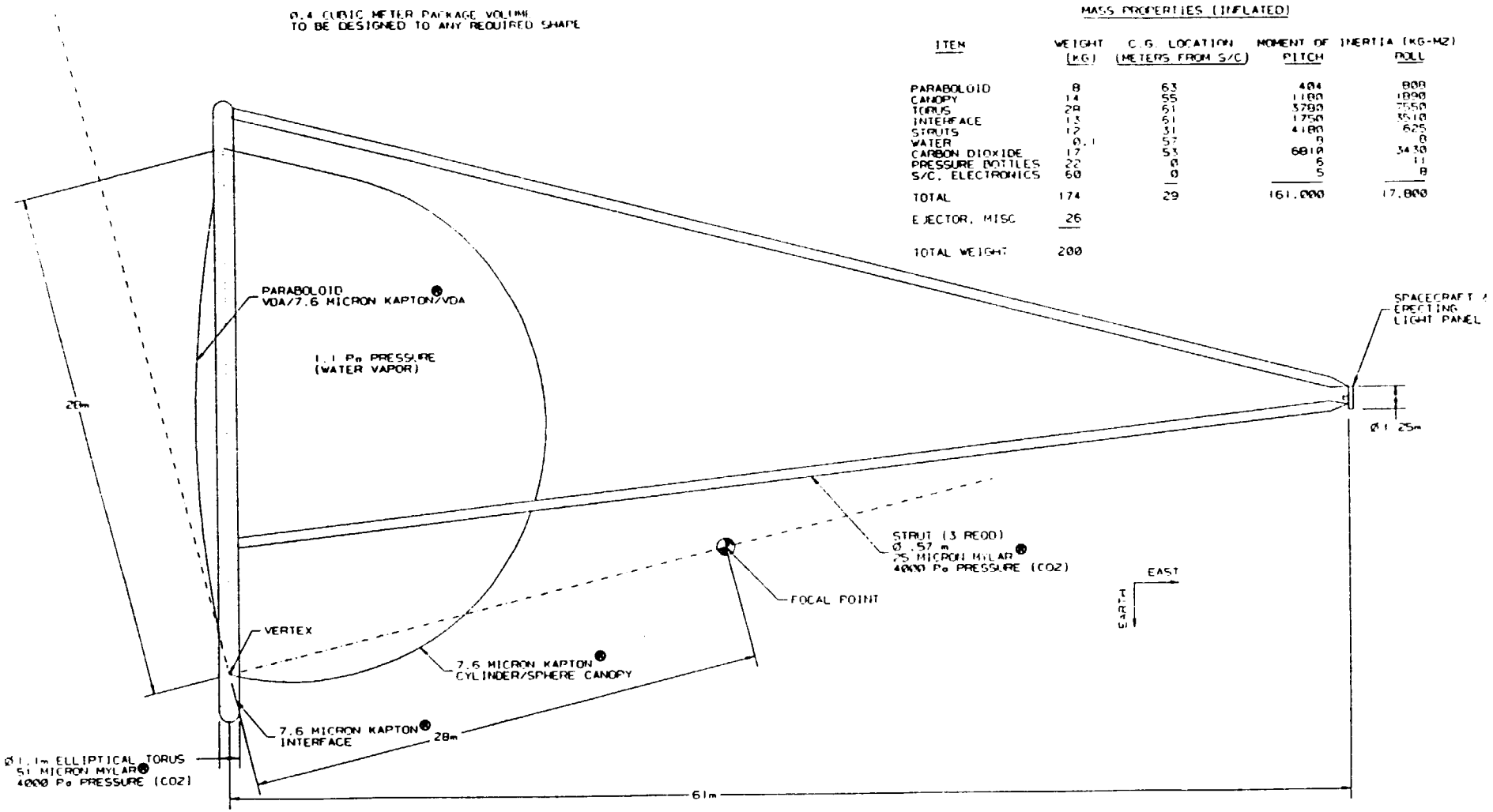

Figure 19. Deployed Large Inflatable Paraboloid Experiment

3.1.2 Inflatable

The inflatable consists of a paraboloid and its canopy, its supporting torus, and three struts attaching the torus to the spacecraft.

The paraboloid is made from VDA/7.6 micron Kapton®/VDA thin film, 1.5 meters wide. VDA stands for "vapor deposited aluminum". About 0.15 micron of aluminum will be deposited on each side of the thin film to assure solar opaqueness. The paraboloid gores are precision cut (using aluminum templates) to the flat pattern required by L'Garde's FLATE code. These gores are joined at their edges by 20mm wide, 7.6 micron thick Kapton® tape and compatible adhesive. When the paraboloid is pressurized to 1.1Pa, the resulting stress of 4.5MPa elastically stretches the Kapton® to a true parabolic shape.

The canopy is made of unmetallized 7.6 micron thick Kapton®. Its shape will be a cylinder-sphere so as to minimize the load on the torus. It is constructed in a manner similar to the paraboloid.

The elliptical torus is the main structural element which keeps the paraboloid edges properly located, and which resists the loads produced by the paraboloid and canopy. The peak ultimate loads of 1000N compression and 1300Nm bending moment occur at the major axis ends. These ultimate loads are a conservative 50% higher than operating loads. The torus is made from cylinders 1.1 meters in diameter, taped together to form an ellipse. Each cylinder, made from 51 micron thick Mylar®, has its ends cut at (different) angles for its particular location in the ellipse. (An alternate approach is to vary cylinder length, keeping the end cut angle unchanged. This reduces tooling costs.) Three struts, 0.57m in diameter and made of 25 micron thick Mylar® attach the torus to the spacecraft.

The torus and paraboloid are attached together in a manner similar to that shown in Figure 20 (which is being used on the DSCE paraboloid). The torus and paraboloid will be inflated on the ground, with the paraboloid-canopy section being made weightless by floating it using nitrogen. Then the edge of the paraboloid will be adjusted until it is at the correct dimensions; that is, a flat ellipse. The screws will then be locked in place. An optical system would probably be used to locate the paraboloid edge for adjustment.

3.1.3 Electronics

Along with the accuracy measurement equipment previously discussed, the instrumentation electronics will provide excitation signals to transducers, instrumentation amplifiers, and filters as needed to produce a voltage analog of measured physical phenomena. These signals will go to a multiplexer, sample-and-hold amplifier and analog-to-digital converter. The resulting digitized data will be formatted into a standard IRIG-106 PCM serial stream in randomized non-return-to-zero (RNRZ) format. This data will be filtered and used to frequency modulate a sub-carrier oscillator. Simultaneously, a TV camera will be used to view the deployment. The TV standard video will be fed to the telemetry transmitter.

Both the video and the PCM sub-carrier oscillator will modulate the telemetry transmitter, such that all instrumentation data will be downlinked on

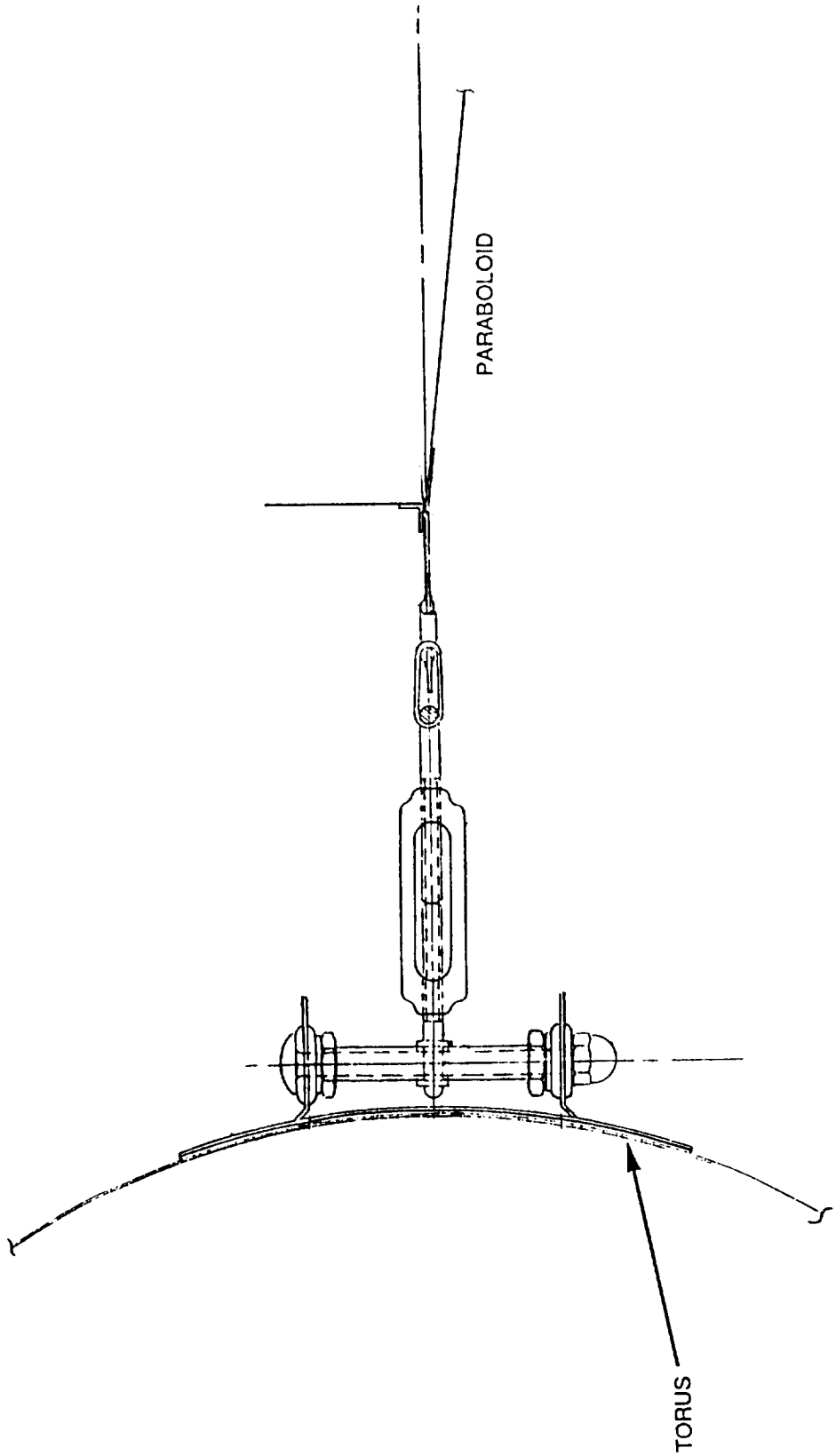

Figure 20. Paraboloid Adjustment Mechanism (Roughly 1000 Req'd)

a single RF link. Because of the relatively wide bandwidth, it is recommended that the downlink be in the 1710 to 1850 Ghz telemetry band.

The deployment sequencing electronics consists of timing circuits and power drivers necessary to activate deployment devices. Gyro-controlled rate stabilization will be provided to stabilize the spacecraft.

All of the above electronics will be operated from a battery pack. The telemetry transmitter, receiver and gas control valves will operate directly from batteries without regulation. The remainder of the electronics will be supplied from appropriate regulators. Note that each light in the accuracy measurement panel will be on less than 7 seconds for the entire flight; therefore, they will not use excessive power.

3.1.4 Gas Sub-Systems

Gas will be used for initial spacecraft control, inflation, and dynamic disturbance. After release from launch vehicle, the spacecraft will be oriented roughly parallel to the earth, and its rates will be minimized. This will be done with a tiny gaseous nitrogen supply, solenoid valves and nozzles. This system may also be used during the inflation process to remove a differential roll rate between the inflatable and spacecraft. This subsystem probably would not be used after inflation.

An operational inflated antenna would use self-rigidizing struts and torus because replacement gas would be prohibitively heavy for a structural system with a ten year life. For this LEO experiment, pressurized struts and torus are used to reduce experiment cost. The required internal pressure is approximately 4000Pa. Conceptually, carbon dioxide (CO_2) has been selected for safety and low weight. While CO_2 is heavier than other gases, it is stored as a liquid and therefore, requires less volume and pressure bottle weight. At room temperature, CO_2 vapor pressure is only 5.8MPa. Therefore, the bottle burst pressure need only exceed 50MPa. For gaseous nitrogen, bottle burst pressure would have to be at least 165MPa for a similar package volume.

It will take up to 4MJ to vaporize the 17kg of CO_2. There is sufficient energy in the CO_2, its pressure bottles and the thin film to accomplish this. However, the CO_2 will be metered out slowly, allowing the sun and conduction to minimize the temperature drop. Cylindrical CO_2 bottles will be mounted externally on the spacecraft and manifolded together.

The paraboloid-canopy volume is filled from a small water bottle and solenoid valve located on the torus. With reserves, only 100 grams of water is needed. When the valve is opened, the water vaporizes and is fed to the paraboloid. Pressure is measured by a simple rheostat-like device that measures the distance that a gore centerline bows out relative to its taped edges. For experiment simplicity, possibly the torus 4000Pa gaseous CO_2 will be used instead of a separate water supply.

For the structural dynamics test, solenoid valves and nozzles will be located on the torus to provide an impulse to the system. The torus gaseous CO_2 will be used as the propellant.

3.1.5 Structure

The spacecraft will be made primarily from aluminum and plastic. The inflatable thin film will be packaged forward of the spacecraft, and covered with three hinged pie shaped doors. The doors may be plastic to reduce telemetry antenna pattern distortion. On orbit, the doors will be opened and locked. They provide a platform for additional lights should a 1.25m diameter spacecraft footprint not be available.

3.2 EXPERIMENT APPROACH

The experiment planned involves the stabilization, erection, and accuracy and structural-response measurements of the inflatable parabolic off-axis reflector previously shown in Figure 19. The experiment package consists of the inflatable and a module. The system is fully instrumented with all of the supporting electronics being housed in the module. The instrumentation monitors all of the experiment events and measures the pertinent parameters. This information is then downlinked real-time to ground stations via a telemetry system in order to conduct post-flight analyses.

The launch vehicle will carry the experiment package containing the inflatable and its supporting subsystems to an orbit above 400km perigee. Power is turned on and all electronic systems are activated. It will be ejected at a pre-known direction and time. The package will be stabilized via its control system. Once the package is stabilized, the inflatable is exposed by opening the containing doors. This is immediately followed by inflation. Since the struts and torus form one large cavity with the struts being the inflatant conduit, the struts will inflate first, then gas will flow into the torus until the 4000Pa pressure is attained in both. The reflector is then inflated.

Since this experiment is being conducted at low altitude, atmospheric drag must be considered. Fortunately, due to the system geometry which places the center of gravity far away from the center of pressure, the natural stability of the configuration is for the reflector to trail the module along the orbital path. Therefore, drag will naturally orient and stabilize the system -- maintaining the struts in additional tension and the reflector pointed in a direction parallel to the Earth's surface. With the system stabilized, the measurement of the reflector accuracy and the system structural response can be made.

A video camera is the prime instrumentation used to fulfill all three objectives validating the erection process, measuring the reflector accuracy and measuring structural dynamics. A wide angle will allow viewing the reflector together with the struts while a narrow angle will cover solely the reflector. Video coverage of the inflation is critical in order to ascertain the completion of a successful inflation and to monitor the experiment, verifying the environmental conditions and identifying any anomalies.

After inflation is complete and the system stabilized, the surface imager (discussed earlier) is activated. This consists of an array of lights mounted on top of the module which illuminate the reflector and whose reflection is viewed by a video camera. Each light on the array is lit for a second in a specific order and its pattern of reflection is seen through the camera and thus recorded. The reflector accuracy can then be determined during post flight data reduction and analysis.

Inflatable structures are dependent on pressure for rigidity and surface accuracy. therefore, measurement of the pressure in the torus and strut cavity as well as the reflector is important. The torus and struts cavity will be inflated to its nominal pressure to establish a rigid structure throughout the experiment.

Paraboloid accuracy will be measured for at least the following conditions. Complete measurement for one set of conditions takes about 100 seconds.

Case	Inflation Pressure	Approx. Sun Angle (Degrees from Base Centerline)	Terminator
1	Low	0	N/A
2	Nominal	0	N/A
3	High	0	N/A
4	Nominal	30	N/A
5	Nominal	60	N/A
7	Nominal - Low	None	Just prior to In/After

Upon completion of the accuracy measurements, a structural dynamics experiment shall be performed to verify the structural response of the system perturbations. Specifically, it is desired to see the impact of external disturbances on the reflector accuracy. Therefore, two torus mounted thrusters are fired to provide an excitation impulse and the reflector response monitored using the surface imager and strain gages on the paraboloid.

The three objectives of the experiment are thus accomplished with each parameter being measured and telemetered to ground stations for post-flight analysis.

3.3 GROUND OPERATIONS

The antenna array and spacecraft will have been tested, prepared and packaged for use at least four months prior to the mission.

Ground operations prior to launch consist of checking payload health, loading the payload (antenna array/spacecraft) into the carrier vehicle and verifying the payload separation system. Needed at the launch site are a) a small checkout space, b) payload hoisting equipment and personnel, and c) integration services.

In addition to the above effort associated with the payload, the ground tracking and telemetry downlink equipment and facilities must be verified. The ground station and associated personnel would have to be government supplied.

Government post mission ground operations consist of securing the telemetry-tracking sites from their activity and properly marking the recording media and preparing it for transportation to a central data processing and analysis site.

3.4 FLIGHT OPERATIONS

The carrier vehicle must be stabilized. An orbit with a perigee of no less than 400km is required; lower perigees will result in excessive drag on the inflatable. An eject signal needs to be supplied. The approximate orientation (± 30°) of the experiment at release should be pre-determined. Ground facilities must be provided for receiving and recording telemetry downlink data. Recording for standard video (RS-343) and PCM digital data will be required.

The number of ground tracking stations will depend on final definition of the intended orbit. It is recommended that at least two telemetry tracking stations be available for recording downlink data and that these stations be separated by at least several hundred miles to avoid loss of data due to anticipated nulls in the spacecraft antenna radiation pattern.

3.5 DATA REDUCTION AND ANALYSIS

The surface imager is the major instrument for the experiment. Data are gathered by a video camera. For each light that is lit, data reduction is done by digitizing a video frame picturing the antenna. If an xy position on the antenna appears to be lit, it is known that a ray from the light has hit the antenna surface and was reflected to the camera position. Thus, the exact position of the surface normal vector at that point is known. By similarly reducing the data from a different light, a different set of surface normals is found. The total set of surface normals thus found is fit to a smooth surface which can then be compared with the desired paraboloid. Included in the result is the paraboloid accuracy expressed as one value.

3.6 FLIGHT JUSTIFICATION

Accomplishment of the three prime objectives for the flight of the large inflatable antenna require space flight:

1. Validate erection of a packaged 28m off-axis parabolic antenna.

2. Determine surface accuracy of the paraboloid as a function of internal pressure and sun aspect angle.

3. Determine the structural dynamics of a large inflatable.

The erection of a large inflatable must be carefully controlled. A thin film can weigh as little as 10 grams/square meter so it accelerates at a high rate under what may seem to be an insignificant pressure. The film's kinetic energy due to the resulting film velocities must be absorbed by the film as strain energy at full erection. If that kinetic energy (or velocity) is too high, the inflatable will rupture. These areas require careful engineering, but no breakthroughs.

To meet this objective, a space environment is mandatory. A space inflatable of this size must be erected in a vacuum because it takes 100,000 times more gas to inflate in the atmosphere than in space. It also requires at most micro-g conditions (for a minute or more) since gravity unrealistically helps or hinders erection. The NASA Lewis Zero-G facility provides a vacuum free fall time of only five seconds for objects less than 6 meters in diameter, much less than the requirements for 28 meters for over a minute.

Fulfilling the second objective will result in invaluable data in a realistic environment. To date, the accuracies of 3m antennas have been measured on the ground, and have been found to be sufficiently accurate for frequencies up to 10Ghz. The accuracy of a 9m off-axis antenna is currently scheduled for ground test measurement. The proposed flight experiment will provide accuracy data for the first time a) of a large antenna b) in space c) at different solar aspect angles. Data will also be gathered at different inflation pressures as has been done on the ground for small antennas. Fulfillment of this objective will provide most of the data needed to prove the credibility of space inflatable antennas and quantify the maximum useful frequency.

The second objective also requires a space environment primarily because of its size. As antenna size increases, required inflation pressure decreases because the radius of curvature becomes large and a low inflation pressure is essential. The optimum differential pressure for the 28m antenna is only 1.1Pa, five orders of magnitude below atmospheric. Clearly normal atmospheric pressure is continually changing more than 1.1Pa, so a sealed chamber at least 28 meters in diameter, would be needed to test on the ground. The test may be adversely affected by gravity pulling on the paraboloid, as well as by the need to maintain an infinitesimal differential pressure on the ground rather than an absolute pressure in space. Finally, testing in space is obviously more realistic for a space antenna.

The third objective is to determine the structural dynamics of a large inflatable containing gas at low pressure. An inflatable antenna will be less accurate and possibly unusable for a period of time after a disturbance such as the use of a reaction control subsystem. Smaller, higher pressure inflatables damp within a second per ground tests. With the data from this proposed experiment, the dynamics can be more accurately modeled, and of course, the raw data will provide a damping curve for a realistic point design.

The third objective also cannot be accomplished on the ground. Floating the inflatable requires gas on both sides of the paraboloid and canopy, and at significantly larger pressures than the operating pressure in space. These unrealistic, higher pressures would be the prime factor in damping the inflatable. If the inflatable were hung in a vacuum chamber, the chamber would have to be evacuated to considerably less than 1Pa. Even if this is accomplished, gravity would still affect damping. A space environment is mandatory.

3.7 STATEMENT OF WORK

The following specifies the tasks required to complete this flight experiment.

3.7.1 Scope and Objective

This Statement of Work (SOW) delineates the tasks required of the contractor responsible for providing the hardware and documentation for the flight experiment, integration and test range support, postflight data reduction, and the final report. The prime objectives of the experiment are 1) to validate erection of a large inflatable, 2) to measure paraboloid accuracy suitable for frequencies up to 10GHz, and 3) to measure the structural dynamics of an inflatable under low pressure.

3.7.2 Background

NASA and the military have urgent needs for large space antennas and collectors. Work performed during the past decade have demonstrated that the weight and cost of mechanically erectable antennas are prohibitive especially for the larger systems and lower frequencies. Inflatable antennas, however, have been demonstrated on a small scale to be suitable for most frequencies (<10GHz) and lifetimes (5-10 years) at weights, package volumes and costs about an order of magnitude less than mechanically erectable systems. Ground testing of large antennas is limited because of the presence of gravity and the lack of sufficiently large vacuum chambers. Hence, critical data can only be obtained in space.

3.7.3 Compliance Documents - All Phases

The contractor shall comply with the "Applicable Documents" as specified in "Appendix C Applicable and Reference Documents" of Announcement of Opportunity, NASA A.O. No. DAST 1-89, November 1, 1989.

3.7.4 Contractor Tasks - Phase I

The contractor shall accomplish the following tasks per the schedule of 3.8.

Studies and analyses shall be performed to support experiment definition and preliminary design. These shall include but not be limited to a) launch and on-orbit environment definition, b) launch and on-orbit structural and thermal analyses, c) power and gas requirements, d) command and control functions and requirements, e) mass properties (packaged and erected), f) paraboloid gore definition.

Preliminary experiment planning shall include, but not be limited to (a) the development of on-orbit time lines (b) calculation of drag and altitude versus time, (c) definition of ground station requirements and pre-launch checkout requirements, (d) preparation of a manifest request.

A system safety program shall be established and maintained. Launch vehicle safety requirements shall be reviewed. Pyrotechnics, pressure bottles and other potentially hazardous components will be selected or designed to meet requirements. Ejection analyses shall be performed to determine worst case envelopes. A preliminary failure modes and effects analysis shall be performed to determine potential hazards to the launch vehicle. Phase 0 safety documentation shall be prepared.

Preliminary design layouts shall be prepared of the packaged and inflated configurations. All components shall be identified, and preliminary make/buy decisions shall be made. Preliminary interface control drawings shall be prepared. Technologies critical to the success of the program shall be demonstrated.

Up to two formal reviews, a conceptual design review and a preliminary design review shall be conducted.

3.7.5 Contractor Tasks - Phase II

The contractor shall accomplish the following tasks per the schedule of 3.8. Analyses shall continue primarily in support of detailed design, development testing and experiment planning.

Detailed drawings and parts lists of development test hardware, factory support equipment and the flight unit shall be prepared. The drawing schedule shall be phased to emphasize parts and subassemblies needed for development testing.

Development test hardware shall be fabricated. Test items shall be made from flight hardware drawings unless impractical. Development tests shall be conducted on all subsystems. These tests shall include but not be limited to (a) ejection, (b) thin film and related bond mechanical properties, (c) thin film inflated structures load carrying capability, (d) sub-scale paraboloid accuracy, (e) large scale vacuum erection, (f) control subsystem, (g) flight optical instrumentation, (h) torus-paraboloid jointing, (i) telemetry operation and antenna patterns, (j) critical environments. The detailed drawings shall be modified to reflect the results of development testing.

The safety program started in Phase I shall continue. Safety issues and questions shall be submitted to NASA as they arise. Safety data packages shall be prepared and submitted.

Integration data including the payload integration plan, shall be furnished to NASA in a timely manner. Integration meetings shall be supported. Integration includes payload-launch vehicle, pre-flight ground support, flight support, and telemetry ground station support.

A Critical Design Review (CDR) shall be held at the conclusion of detailed design and development testing. The contractor shall show evidence that the design will operate successfully and safely from fabrication through on-orbit testing.

The flight hardware shall be fabricated and assembled using the in-house configuration management and quality assurance (QA) programs approved by NASA. QA shall also witness all testing conducted during fabrication and assembly. All such testing shall follow written detailed procedures. The flight unit shall be subjected to critical environments approved by NASA. These shall include thermal-vacuum, modal survey, EMI/EMC, subassembly leak tests, vibration, mass properties and launch loads. The contractor shall support a flight readiness review at the conclusion of all testing.

The contractor shall support pre-flight operations, including health checks and integration, and launch. The contractor shall operate the experiment under the authority of NASA. The contractor shall collect and reduce the flight data, and publish a final report in NASA format providing a full summary of the experiment and its results.

Throughout the phases, the contractor shall manage the program, assuring that the tasks are completed within cost and schedule. He shall provide monthly written and/or oral data reviews to NASA.

3.8 SCHEDULE AND COST

The milestone schedule shown in Figure 21 shows that there is 5.3 years between go-ahead and flight. This probably could be reduced by a year, if necessary, with no increase in cost.

The total cost of the experiment (excluding launch and other government support) is expected to be $5M. Most of the funds are needed in the first three years.

Phase I (1 year)	$1.4M
Phase II (1st year)	1.2M
Phase II (2nd year)	0.9M
Phase II (3rd year)	0.6M
Phase II (subsequent)	0.9M

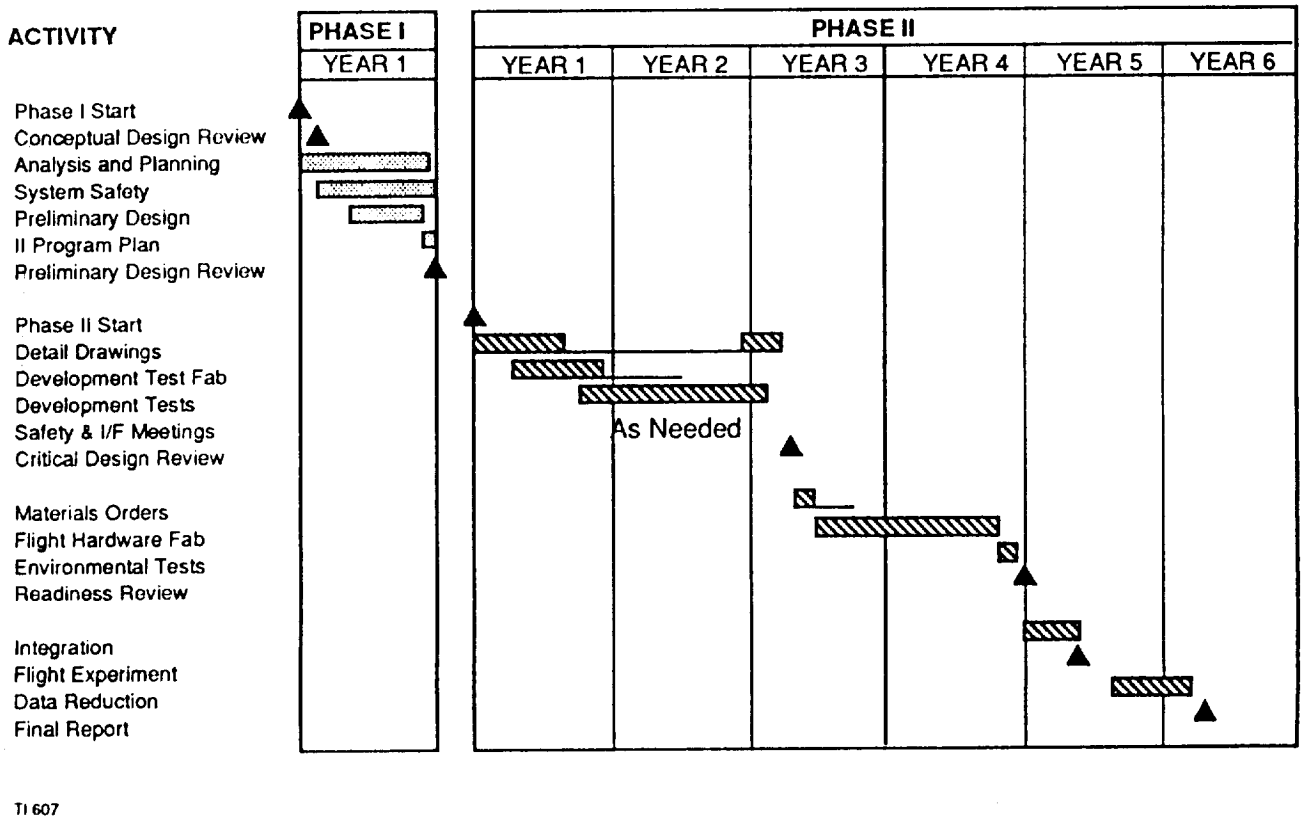

Figure 21. Schedule

4.0 METEOROIDS

One concern with any structure in space is the effect of impact with particles. Although the majority of particles are very small (with diameters on the order of microns), their velocity can be up to 20 kilometers per second; the energy of impact is immense.

These particles are divided into two classes; natural and man-made. Natural particles (meteoroids) most commonly originate from comets, while some of the of the larger particles are actually asteroids revolving about the sun. The majority of these meteoroids have diameters in the 1-100 micron range. The man-made debris consists of space craft paint flakes, expended rocket stages, rocket panels, nuts and bolts, and even hand tools that have slipped from the gloves of space-walking astronauts. Without a doubt, the space around our planet is polluted, which increases the concern of spacecraft damage. This study provides meteoroid models for both low earth orbit (LEO) and geosynchronous earth orbit (GEO) in Section 4.1.

Ground test data and analyses were used to predict the damage done to inflatables in space (Section 4.2). Figure 22 shows the results at GEO for four materials with thicknesses up to 50 microns. Hole area increases with film thickness over the range shown, but will eventually reduce to zero as the film becomes very thick. When the meteoroid hits a film, it fragments. If the film is thin relative to the meteoroid diameter, the resulting hole diameter is equal to or slightly greater than the meteoroid. As the first film gets thicker, the fragments are able to do more damage to the first film, and the resulting first film hole can be several times the meteoroid diameter.

The very limited test data indicate that meteoroids are unable to penetrate a second film if they create a large hole in the first film. If the meteoroid leaves a small hole in the first film, its fragments have the energy to do extensive damage to the second film. Unfortunately, there is insufficient data to model second film damage.

Figure 23 shows the frontal area of the larger meteoroids that are capable of penetrating the second film. In one test, a particle created holes in the second film sixty times larger in area than that of the particle.

Meteoroid impact is especially important for inflatables, since the gas which holds the shape of the structure leaks out through the holes created by particle impact, and must be replenished to maintain the correct operating pressure. The weight of the replacement gas is directly proportional to the operating pressure and the hole area. The film should therefore be thin to minimize both operating pressure and first film meteoroid damage. This infers then, that it is best to incorporate internal meteoroid shield(s) to protect against second inflatable film damage rather than to increase the inflatable's film thickness. This has been confirmed for the ESGP concept, and is likely to be true for any inflatable that requires a significant film stress.

The internal shield would be made of thin film identical or similar to that of the inflatable. Sheets would be located within the inflatable such that a meteoroid approaching the inflatable from any direction would have to penetrate the shield before it could reach the second surface of the inflatable. It is believed that two very thin films are superior to one thicker film because the

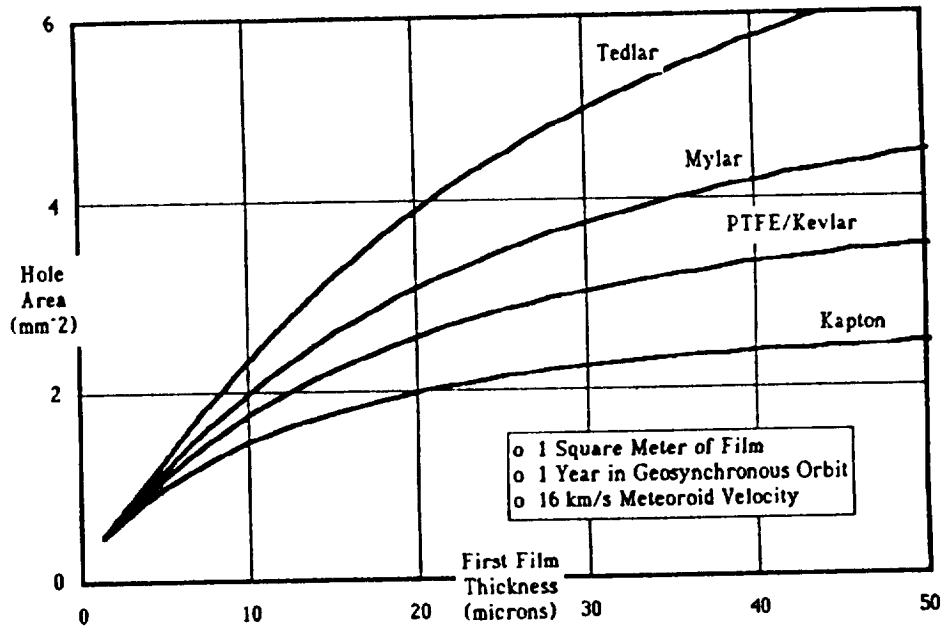

Figure 22. Hole Area Expected in the First Film

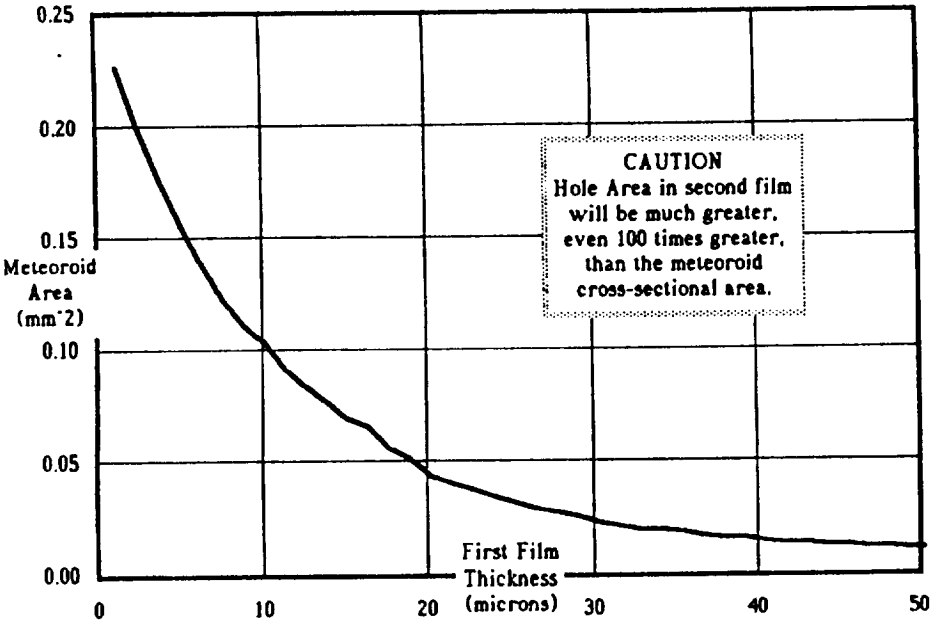

Figure 23. Initial Cross-Sectional Area of Meteoroids Capable of Penetrating a Second Film

meteoroid fragments and the fragments spread each time it hits. The idea is to spread the meteoroid's energy over a larger area, and to reduce the fragments' sizes so that they are small relative to the inflatable's second film.

Sections 4.3 discusses the film stress desired for an accurate paraboloid or collector (4.5MPa), and Section 4.4 discusses the selection of an inflatant low in package volume and weight (water vapor). Knowing these items, one can calculate the replacement inflatant that must be carried in order to replace that lost through meteoroid holes. Section 4.5 derives the inflatant loss equation. For water at room temperature, the total weight (kg) of water lost through the holes in 1 square meter of Kapton® film in one year at GEO is the hole area (mm^2) times the pressure (Pa) divided by 59. For the ESGP concept of Section 2, pressure (P) is 0.25Pa, hole area (A) from Figure 22 is 1.2mm^2, and the maximum projected area of the ESGP is 650 square meters. Therefore, 3.3kg of water is lost in the first year. The total mass loss is proportional to years squared (since holes continue to increase with time). For a five year life, 83kg must be launched with the unit. The conceptual design of Section 2.0 has 91kg. While this is a significant portion of the erectable collector subsystem weight, the overall collector weight (including replacement water) is considerably less perhaps 10 times less, than non-inflatable collectors.

Section 4.6 contains a list of symbols used in the following paragraphs.

4.1 METEOROID ENVIRONMENT

While the flux of particles in space is not constant, NASA-Johnson (Reference 14) has determined design curves for flux vs. mass of meteoroid particles. For this study, two regions were considered--LEO and GEO. More particles are present at LEO due to the man-made debris, and also due to the greater gravitational pull near the Earth; natural meteoroids are actually attracted to the lower orbits by gravity.

First, the population of naturally occurring meteoroids is given in Figure 24 (Reference 14). This curve was generated by telescope observation of meteors (those particles entering the atmosphere), radar observations of meteors, and direct measurements in space (acoustic sensors on spacecraft, etc.). Although the curve was generated twenty years ago, its accuracy is proven again and again by recent spacecraft data.

The effect of the Earth's gravity is given by Figure 25, and is termed a "de-focusing factor." This number is the amount by which the flux in Figure 24 is reduced due to the effect of gravity. For example, the flux at LEO (at roughly 1 Earth radii from the Earth's center is exactly the flux given by the Figure 24 curves. The flux at GEO is this same flux multiplied by 0.63. Again, these design curves are for natural particles, and do not include the more prevalent man-made debris. To convert these curves to flux vs. diameter, NASA recommends a spherical meteoroid model with a specific gravity of 0.5.

The velocity of meteoroids varies widely. Geocentric meteoroid velocities have been observed in a range from ~10 to ~75 km/s, with a high probability that the velocities will range from 10 to 30 km/s. Many previous studies have used an average velocity of 16 km/s, which will be used here.

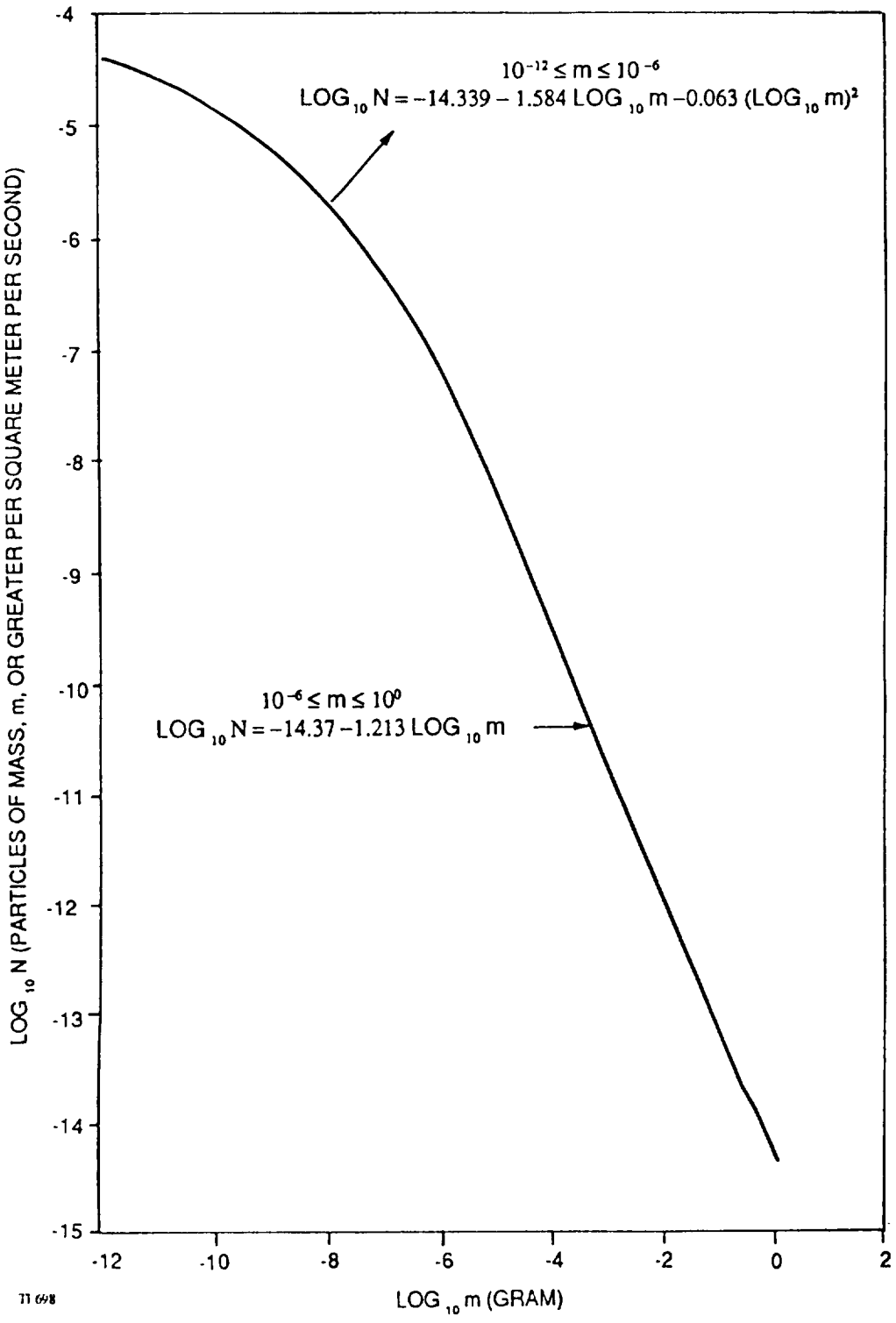

Figure 24. Average Cumulative Total Meteoroid Flux-Mass Model for 1 A.U.

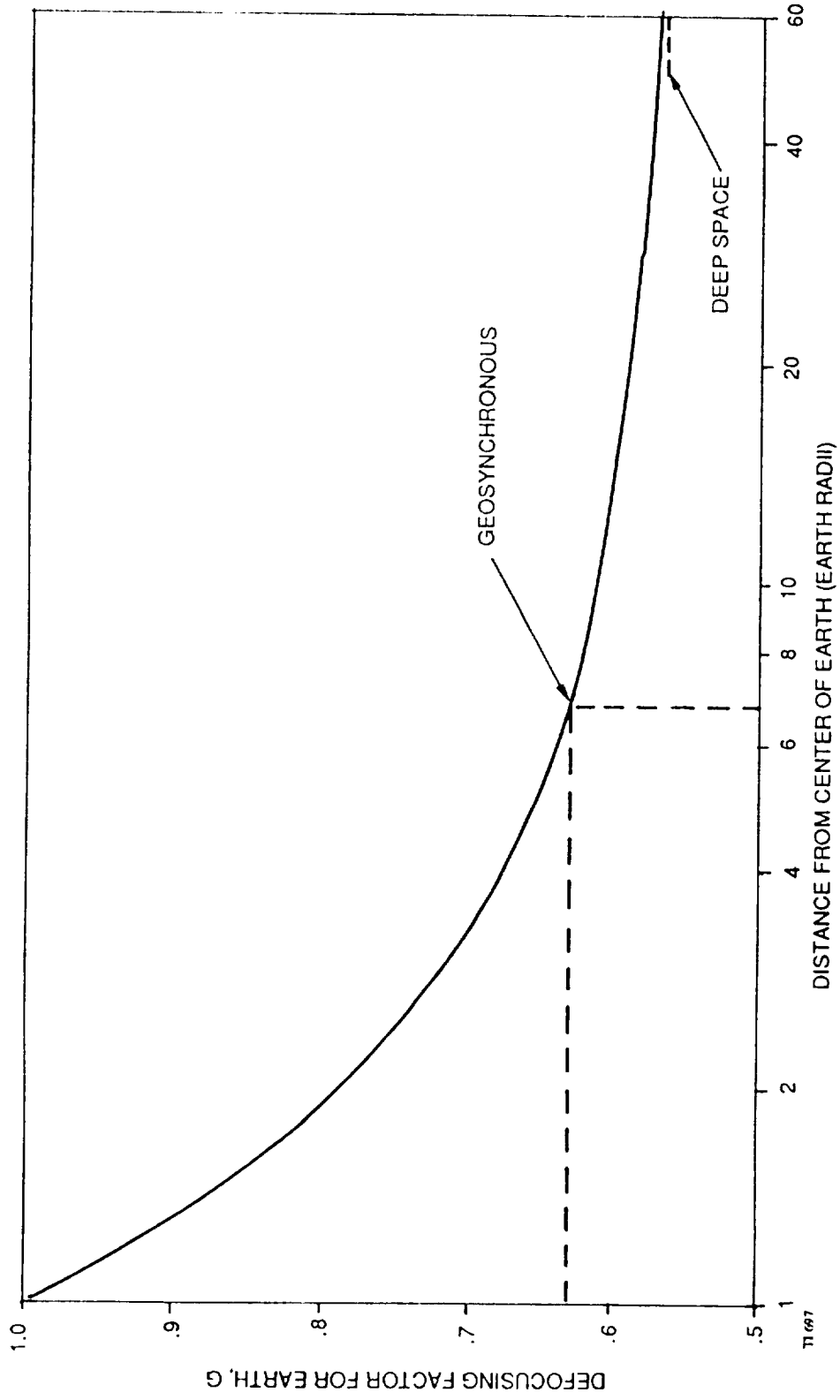

Figure 25. Defocusing Factor Due to Earth's Gravity

It became evident in the late 1970s that spacecraft debris in low earth orbits was becoming a more serious threat than extraterrestrial meteoroids. Figure 26 depicts a 1978 estimate of the problem (Reference 16). According to Don Kessler of Johnson Space Center, the data available by early 1985 indicate that the incidence of this debris in the size range below a few centimeters is increasing at a rate much greater than projected in 1978 and has already reached the level predicted for 1995 (in Figure 26). One such set of data was presented as a result of a recent study conducted by the Massachusetts Institute of Technology's Lincoln Laboratory, which employed optical telescopes to look for objects in the size range above 1 cm (Reference 15). For this reason this L'Garde study assumed that the debris population is somewhere between the curves for 1990 and 2020. Curve fits were made for these using a linear regression routine; Equation 1 gives the results for flux vs. mass for the man-made debris:

$$\text{Log } N = -12.1216 - 0.670567\,(\log m) + 0.0599594\,(\log m)^2 + 0.0105698\,(\log m)^3 - 0.000725\,(\log m)^4 - 0.000262\,(\log m)^5 \quad (\text{for } -5 < \log m < 6) \qquad (1)$$

where log refers to base 10 logarithms.

The following equations are used for natural particle flux at LEO,

$$\text{Log } N = -14.339 - 1.584 \log m - 0.063\,(\log m)^2 \quad (\text{for } -12 \leq \log m \leq -6) \qquad (2)$$

$$\text{Log } N = -14.37 - 1.213 \log m \quad (\text{for } -6 < \log m \leq -5) \qquad (3)$$

Equation 1 gives the flux for sizes of $-5 < \log m \leq 6$

The debris is much denser on the average than the natural particles; a specific gravity of 3.0 is used for the debris. Also, since the debris originates from orbiting spacecraft rather than from outer space, its velocity is less--10 km/sec.

Table 4 summarizes the model used for LEO, where the flux is as given in Figure 26.

4.2 HYPERVELOCITY DAMAGE MECHANISM

Equations 1 through 3 were converted to give the number of meteoroids as a function of diameter instead of mass. The distribution can then be divided to find the flux within certain size ranges. The number of meteoroids in a particular size range that hit the reflector is then given by:

$$\text{Hits} = (\text{Flux in that range}) * (\text{Reflector Projected Area}) * (\text{Time exposed}) \qquad (4)$$

To convert the number of hits to the leak area, the relationship depends on the size of the meteoroid. The hole will not simply be the same as the diameter of the meteoroid. The actual relationship is a function of material thickness to meteoroid diameter ratio (T/d), the aspect angle and the material

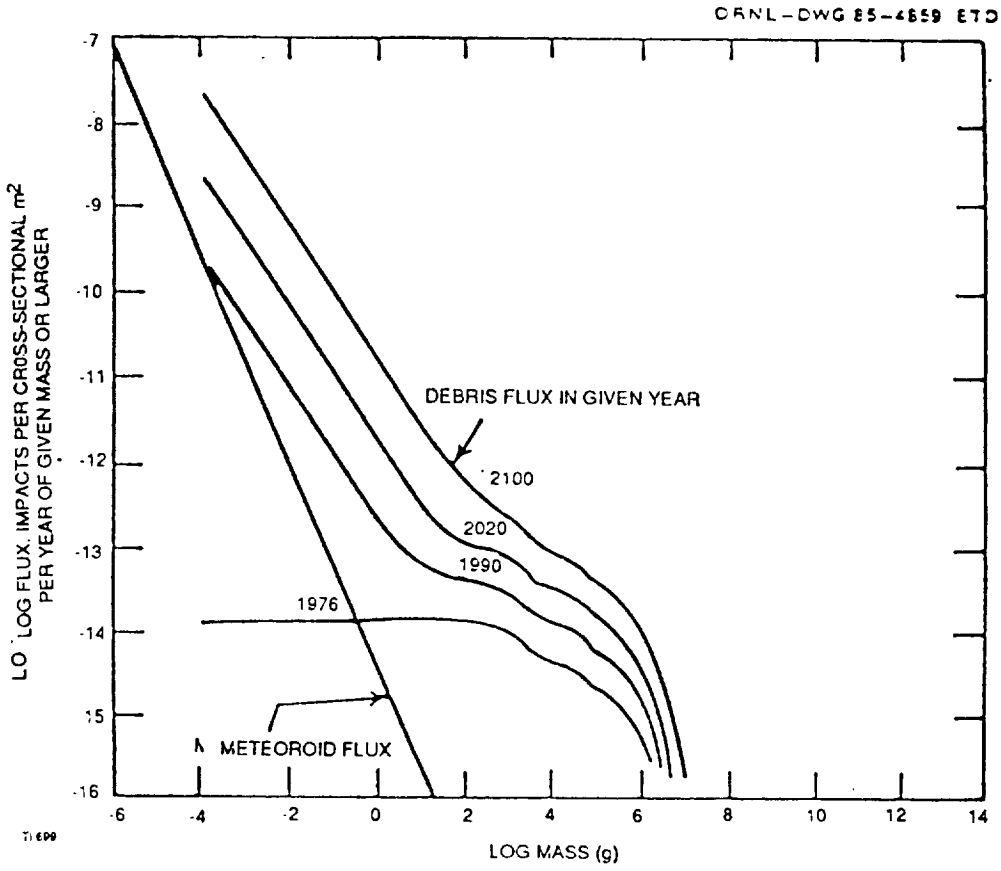

Figure 26. NASA 1978 Estimates of the Flux of Solid Debris Predicted at Altitudes between 700 and 1200 km

of the spacecraft. To simplify the study, it was assumed that all meteoroids approach normal to the surface (90° aspect angle). It should be noted that the individual properties of materials and particles are only slightly understood in their relation to the effect on hole size. The data presented here is based on the few different materials that have been tested.

There are three regimes to be followed based on T/d ratio.

When T/d is small, (ie, large particles, thin film), the particle passes through the material retaining much of its energy. The hole made is only slightly larger than the particle diameter. While passing through, the particle fragments. Since the fragments still have considerable energy, they penetrate the second film of the inflatable. The damage in the second film can be extensive.

In the intermediate range, the meteoroid breaks up into small fragments upon impact with the material. The energy of the meteoroid is not sufficient to cleanly pierce the fabric. Instead, the particle loses kinetic energy by breaking up and perhaps melting or vaporizing the film; these small fragments expand the hole to a diameter that is larger than the meteoroid diameter. The fragments have insufficient energy to puncture a second film.

TABLE 4. SUMMARY OF METEOROID MODEL

Log Mass (g)	Dominated By	Particle Density (gm/cc)	Diameter (Microns)	Velocity (km/sec)	Log Flux (Natural)	Log Flux (Natural + Man-made)
-12	natural	0.5	1.6	16	-4.403	-4.403
-11	natural	0.5	3.4	16	-4.538	-4.538
-10	natural	0.5	7.3	16	-4.799	-4.799
-9	natural	0.5	15.6	16	-5.186	-5.186
-9	natural	0.5	33.7	16	-5.699	-5.699
-7	natural	0.5	72.6	16	-6.338	-6.338
-6	natural	0.5	156.4	16	-7.103	-7.103
-5	natural	0.5	336.9	16	-8.305	-8.305
-4	man-made	3	399.5	10	-9.518	-9.074
-3	man-made	3	860.6	10	-10.731	-9.851
-2	man-made	3	1854.0	10	-11.944	-10.629
-1	man-made	3	3994.0	10	-13.157	-11.403
0	man-made	3	8604.1	10	-14.37	-12.122
1	man-made	3	18535.6	10		-12.723
2	man-made	3	39930.7	10		-13.159
3	man-made	3	86021.4	10		-13.431
4	man-made	3	185313.3	10		-13.622
5	man-made	3	399214.8	10		-13.927
6	man-made	3	860016.2	10		-14.681

In the third range, where the material is much thicker than the meteoroid size, the energy of the meteoroid is not sufficient to pierce the entire thickness of the material. The meteoroid, therefore, loses all of its energy upon impact. The small fragments cause a crater in the material, but there will be no passage of the gas from the inside to outer space.

4.2.1 FRONT FILM DAMAGE

Considerable research and testing has been done to determine meteoroid damage and protection subsystems for satellites. Maiden and McMillan (Reference 17) performed a hypervelocity impact experimental study using aluminum sheets and particles. These experiments were extensive with velocities ranging 1 to 8km/s, and T/d ranging from 0.040 to 0.504. The work resulted in the following empirical relationship which fits the data closely.

$$D/d = 0.45\ V\ (T/d)^{2/3} + 0.9 \qquad (5)$$

where D = hole diameter
d = particle diameter
V = particle velocity in km/s
T = sheet thickness

L'Garde and NASA-JSC both performed hypervelocity impact tests using plastic films as the target. While the amount of data is limited (only 11 tests), the quality appears to be excellent.

The L'Garde tests (Reference 18) were conducted at the AEDC Von Karman Facility Hypervelocity Impact Range S1. The particles were 200 micron diameter Uniform Polystyrene DVB Microspheres with a density of 0.5g/cc -- about that of meteoroids. The targets were 6.4 and 12.7 micron Mylar®, and 12.7 and 51 micron Tedlar®. Particle velocity was 8.44 ± 0.18km/s. Two to five particle hit the target in each of five shots.

The NASA-JSC tests (Reference 19) were conducted at the Johnson Space Center Small Light-Gas Gun (1.78mm bore). Particles were 110 to 210 microns diameter (2.3-2.5g/cc) glass, 127 and 396 micron diameter (4.8g/cc) aluminum oxide, and 396 micron diameter (2.25g/cc) Pyrex. (Only one type and size of particle were used per test.) The target was 76 micron Kapton®. Particle velocities ranged from 5.6 to 6.8km/s.

The results of these two test series are shown in Figure 27. The solid squares and triangles show the test results from References 18 and 19, respectively. For each of the eleven test points, the hole size (D/d) was calculated using the empirical Equation 5 above. These are shown as white squares and triangles at the same T/d's as the test data. In all cases, the actual hole diameters were less than that predicted by the equation. Smaller holes apparently occur in plastic than in hard aluminum.

A new curve fit (using linear regression) was calculated using the same format as that in Equation 5. The result, shown in Figure 28, is:

$$D/d = 0.423\ V\ (T/d)^{0.951} + 1 \qquad (6)$$

where V is in m/s. (The constant, 0.9, in the Equation 5 was changed to 1.0; the former is valid but predicts a hole smaller than that of the particle as T/d approaches zero.)

Hole diameters cannot continually increase with T/d as indicated in Figure 28 because eventually the film will get too thick and/or the particle too small for penetration. No experimental data were found to help define the peak D/d value or the "no penetration" point, so analysis is used.

The maximum D/d ratio is determined by the principle of conservation of energy. The kinetic energy of the meteoroid is considered to be completely converted to heat in melting the film. Actually, this is a conservative assumption, since removal of material would create some vaporization, requiring additional energy.

It is assumed that the crater produced will have a spherical bottom with dimensions as shown in Figure 29.

The kinetic energy of the meteoroid is given by:

$$E_k = \tfrac{1}{2}mV^2 \qquad (7)$$

where m is the mass of the meteoroid and V is its velocity. Substituting in Equation 7 for mass yields the energy as a function of the meteoroid diameter, d:

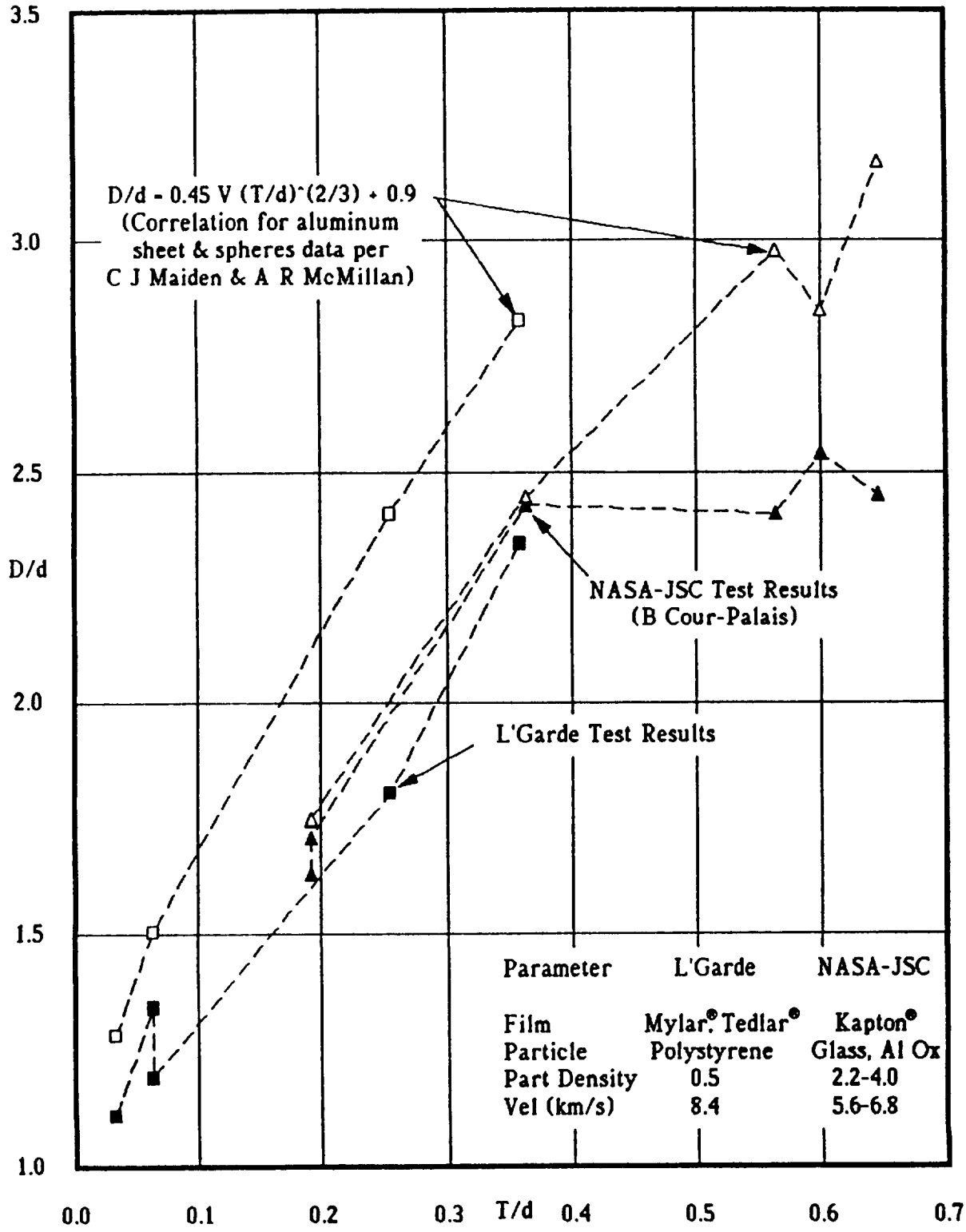

Figure 27. Hypervelocity Impacts on Plastic Films

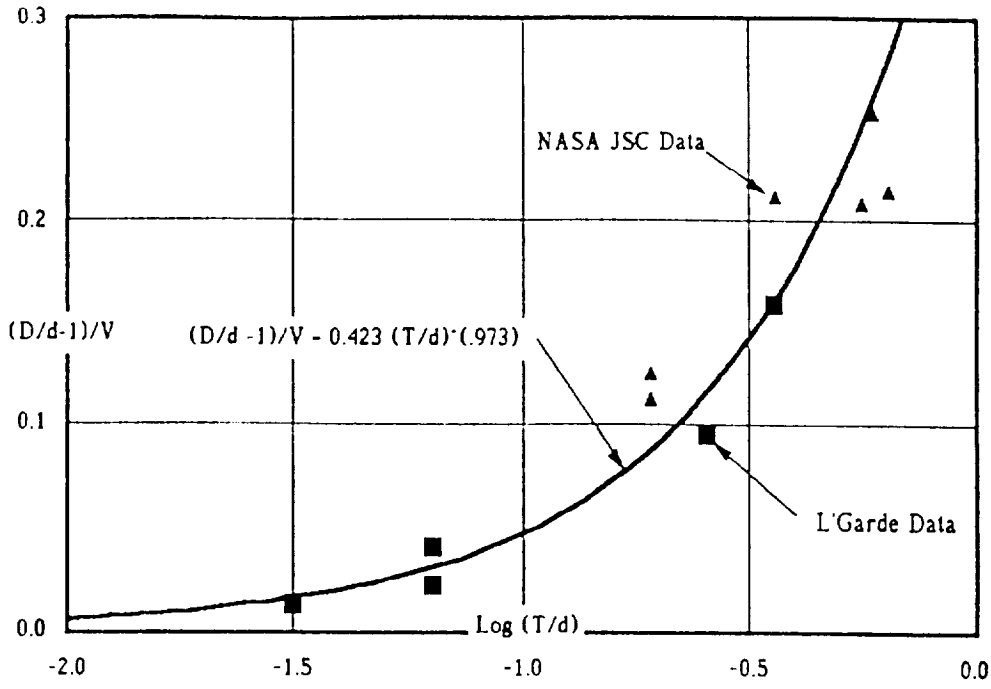

Figure 28. Curve Fit for Hypervelocity Impacts on Plastic Film

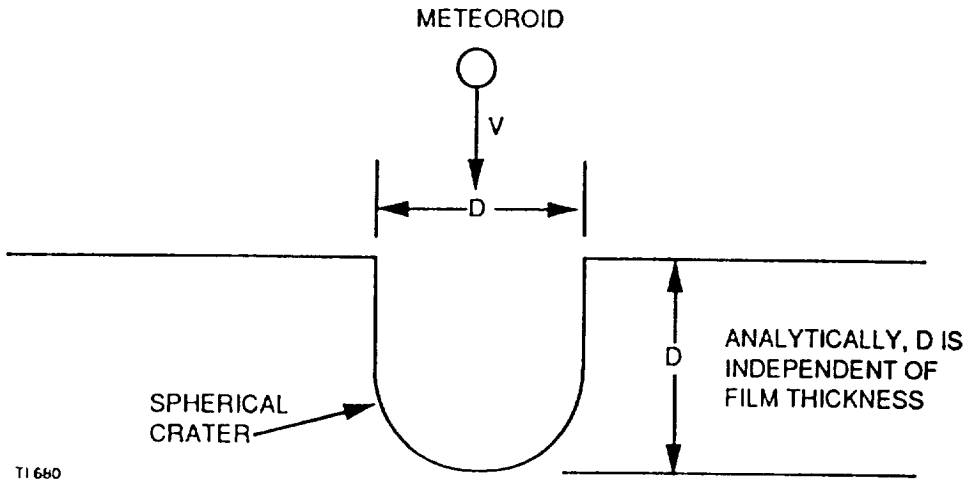

Figure 29. Spherical Crater Formed by Meteoroid

$$E_k = (\pi/12)\ \rho_m\ d^3\ V^2 \qquad (8)$$

where ρ_m is the density of the meteoroid.

The energy required to melt the material in the crater is:

$$E_{melt} = \rho_f\ Vol_c\ h_{melt} \qquad (9)$$

where ρ_f is the density of the film material; $Vol_c = (5\pi/24)\ D^3$; and h_{melt} is the enthalpy required to raise the temperature of the material from an initial temperature T_o, to its melting point and perform a phase change to liquid:

$$h_{melt} = c_p\ (T_{melt} - T_o) + h_{fusion} \qquad (10)$$

where c_p and h_{fusion} are the specific heat and the latent heat of fusion of the film material, respectively.

Equating the energies given by Equations 7 and 8 and rearranging gives the maximum hole diameter to particle diameter ratio:

$$D/d = \left[\frac{2\rho_m V^2}{5\rho_f h_{melt}}\right]^{1/3} \qquad (11)$$

This ratio can be determined for a number of candidate films, based on the heat of fusion, melting temperature, and density of the film. While most plastic films do not melt to a liquid form, they do decompose at high temperatures. Kapton®, for example, reaches a "zero strength temperature" at 1088°K, where the film is useless. Therefore, the heat of fusion is inapplicable in this case. A summary of the material properties and the D/d ratio is given in Table 5. "PTFE/Kevlar®" is a Kevlar® fabric coated with Teflon® to make it leakproof.

TABLE 5. PROPERTIES OF CANDIDATE BALLOON MATERIALS
(16 km/s)

	ρ_f g/cm³	C_p Kcal/Kg°C	Zero Strength Temperature	h_{fusion}	h melt J/Kg	D/d
PTFE/Kevlar®	1.33	0.28	427°C	0	499761	4.25
Kapton®	1.42	0.261	815°C	0	889149	3.44
Mylar®	1.39	0.28	253°C	0	296111	4.99
Tedlar®	1.39	0.24	150°C	0	150480	6.26

The result of Table 5 is the D/d ratio. Its significance is that the damage mechanism follows the curve given by Equation 6 up to a maximum of D/d = 3.44 (Kapton®).

As the thickness/particle diameter continues to increase, the crater will reach a limiting depth and not puncture the material. The limiting thickness per the above analysis would be the crater diameter, or T/d = 3.44 for Kapton®. Note that if penetration is later found to be deeper, the hole size is likely to be smaller.

The results of the preceding are illustrated in Figure 30 for Kapton® film being hit by 16km/s particles. Equations 6 and 11 can be used to obtain similar front film damage models for other films and impact velocities.

After finding the hole diameter produced, the front film leak area can be calculated by:

$$\text{Leak Area} = (\pi/4)(D)^2 \quad (\text{No. of Hits}) \qquad (12)$$

This is done for all particle masses; the results are then tallied, summing up the total number of hits, holes, and total leak area.

4.2.2 Second Film Damage

All inflatables have two film surfaces through which a particle with enough energy could penetrate. The L'Garde tests were conducted with two films in the flight path of the particle. In three of the five tests, the particles penetrated both surfaces. The data is shown in Figure 31 which is plotted for the test velocity of 8.44 km/s since no model yet exists for second film penetration.

Figure 31 shows that the damage to the second film is quite extensive. Some observations from Figure 31 or Reference 18:

a) No second film penetration occurred for the test near Log (T/d) = -0.5. For the lower of these two tests, particle soot was on the second film. This plus the other test data establishes that second film damage stops in the Log (T/d) = -1.2 to -1.0 range (T/d = 0.06 to 0.10).

b) Tedlar® appears to survive second film particle impact better than Mylar®.

c) Insufficient data exists to model second film damage.

The second sheet hole diameters should not continue to increase as T/d decreases. If a bowling ball meteor hit a thin film, one would expect that it would hardly feel the presence of the film. Debris may flake off its surface, but the resulting second film hole diameter should be slightly larger than the bowling ball diameter. It is therefore expected that D/d will increase from zero at T/d $\simeq$ 0.1 to some unknown maximum value and then decrease to slightly more than 1 at a lower value of T/d. More test data is needed in the T/d = 0.1 to 0.001 range.

7.6 micron film is used in the ESGP operational system, so particles greater than 80 microns are a threat. Using Section 4.1 data, 744 meteoroids hit each square meter of an object at GEO annually, creating holes in 0.3-mil Kapton® totaling 1.2 square millimeters in area. Only 1% of these hits are from

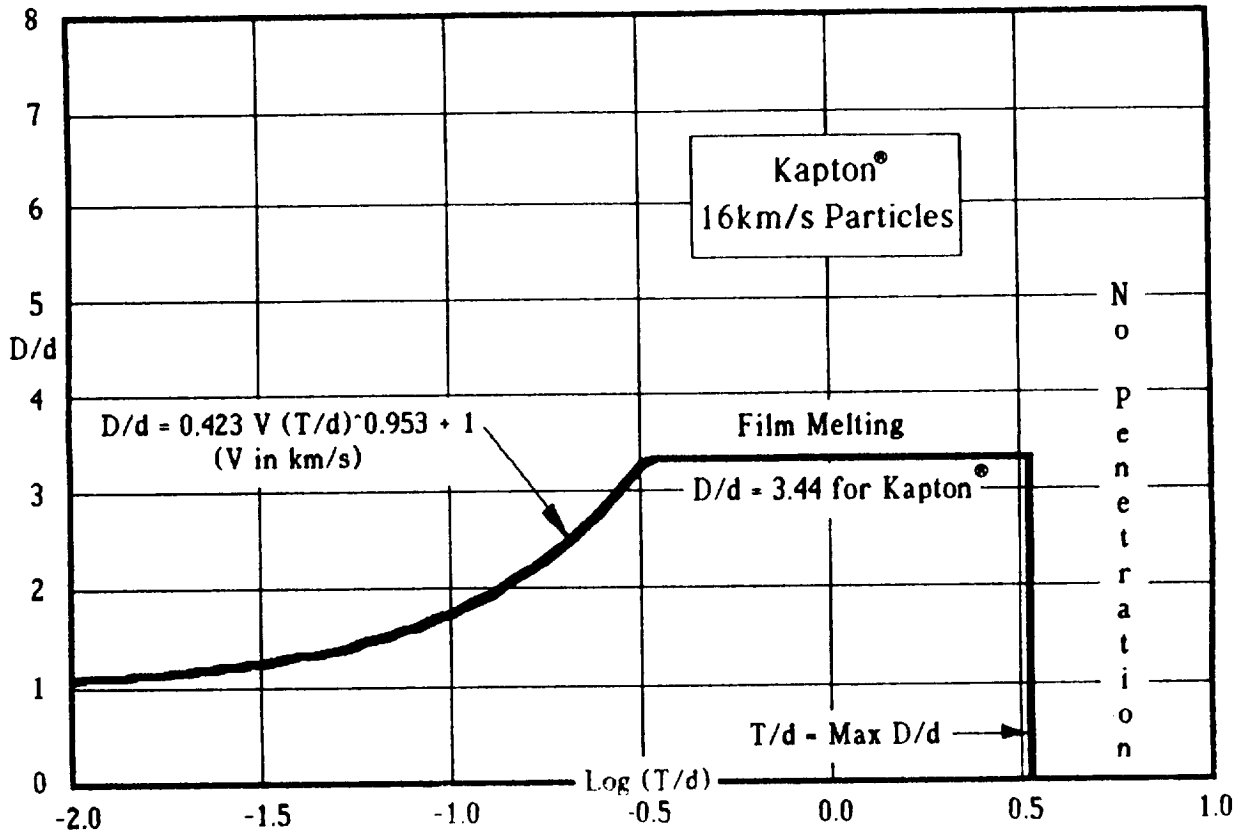

Figure 30. Estimated First Film Hole Sizes Produced by Meteoroids

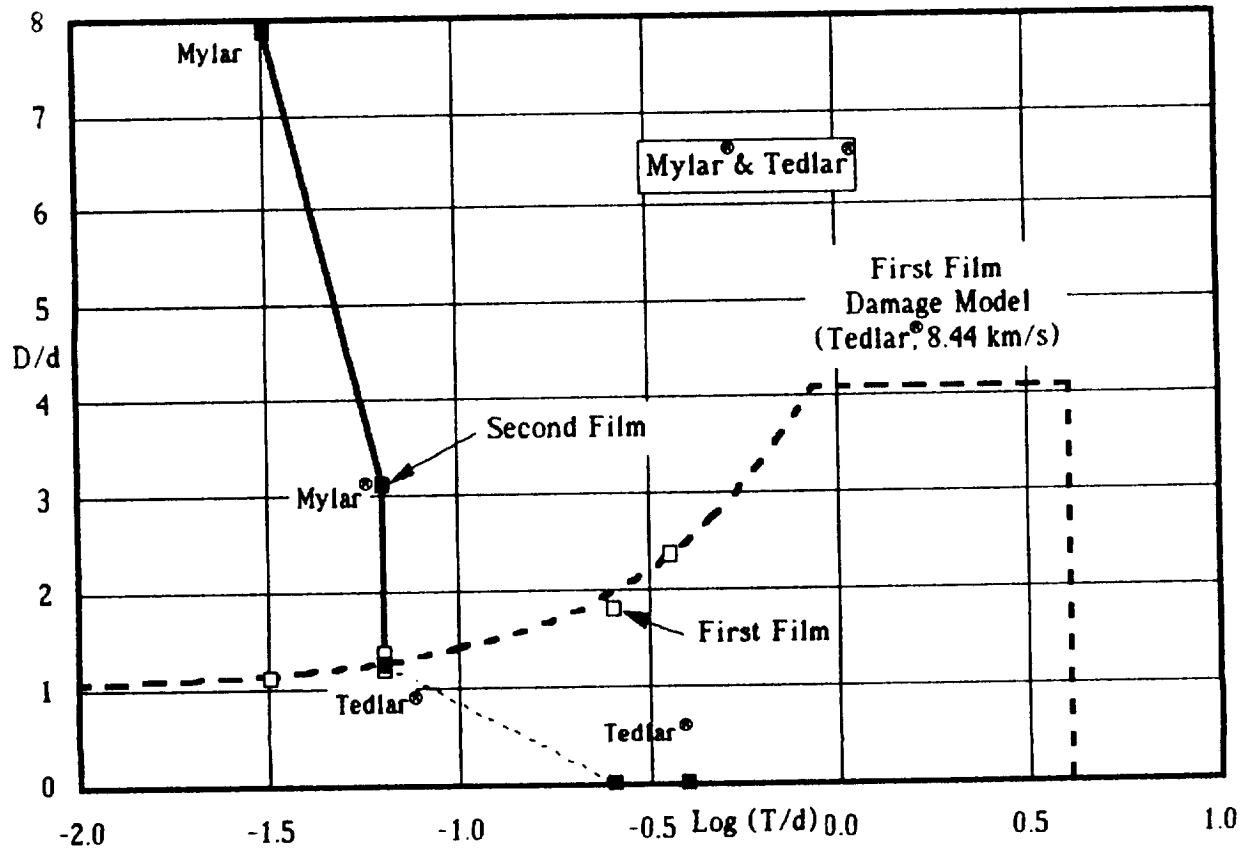

Figure 31. Second Film Damage Produced by 8.44 km/s Particles

meteoroids bigger than 80 microns, but they can cause significant damage because they are bigger. Figure 23 showed that these larger meteoroids total 0.13 square millimeters in area; therefore, they would produce damage exceeding that in the first film if D/d is greater than 3. Since Figure 31 indicates that D/d in the first film could be 8, the design must be modified to handle this increased threat.

4.2.3 Effect on Space Inflatables

An inflatable design with a long life requirement needs to accommodate the possibility of being hit by the larger meteoroids that create holes in the second film. The solution that first comes to mind is to increase the film thickness to, say, 25 microns. The reflector and canopy weigh very little so the resulting penalty is not severe. Only meteoroids greater than 250 microns would then damage the second film. The number of hits from such particles would reduce to less than 0.2 (from 7.4) per square meter per year. This a workable solution but not necessarily the best because a) the gas pressure would probably have to be increased to accommodate the increased reflector thickness, and b) a D/d of 8 is not necessarily the largest hole produced in the second film.

A lighter weight and more certain design solution is to build a meteoroid shield within the reflector-canopy space. This would consist of three planes of thin film, each of which is at a 90° angle with respect to the other two. This internal structure could be made of thin film, so its total weight would be less than that of the reflector-canopy. A meteoroid entering the inflatable would not reach the other side of the inflatable because the meteoroid would always impact the shield. The data shows that meteoroids fragment upon hitting the first film, and the fragments are slower and smaller when they hit the second film. They will again slow and break up when hitting the second film. It is unlikely that they will be able to penetrate a third film because they should be too small and spread out. Also, the shield is at a different angle to particle trajectory than the first shield; therefore, the effective thickness of the thin film is greater than what was assumed for this analysis.

For the ESGP concept, the paraboloid and canopy weight 22kg. A 7.6 micron meteoroid shield adds 14kg. For more conservation, the shield could consist of two layers of thin film at an additional 14kg weight penalty. This virtually guarantees no damage to the second inflatable film since now the meteoroid would have to pass through no less than 30 microns of film, actually much more when attack angle is considered.

4.3 PARABOLOID INFLATION PRESSURE

To determine the gas leakage through the holes, it is necessary to know the inflation pressure. This is set by the stress in the membranes necessary to remove the packaging wrinkles and provide the necessary reflectance.

To develop a smooth reflective surface, it is necessary to determine the stress level that removes the packaging wrinkles in the film. Work from a previous L'Garde contract (Reference 20) showed that the film stress necessary to remove packaging wrinkles in inflatable objects is 4.48MPa (650 psi). This was determined by inflating three test cylinders made of 6.4 micron (0.25 mil)

Mylar®, 7.6 micron (0.3 mil) Kapton® and 41 micron (1.6 mil) Tedlar®, respectively, and calculating the film stress at the point of acceptable reflectance. It was also found that this film stress must be maintained or else the packaging wrinkles will reappear when the pressure is lowered. The only way to permanently remove the wrinkles is to bring the film to its yield stress, which has two drawbacks. First, this added film stress will raise the design requirement and dictate a larger and heavier torus. Secondly, upon inflation the film will be stressed past the material's yield point and plastically deform. When the pressure is then lowered to its operating levels, the reflector possibly will no longer form the paraboloid shape. Thus, for the fully inflated reflector design, a pressure should be maintained permanently that will create a film stress of 4.48MPa (650 psi).

To determine this critical inflation pressure in the reflector, the film stress will be calculated at the point of minimum stress. For an on-axis paraboloid, this occurs at the vertex or center of the dish.

The stresses in the meridional and hoop direction respectively are given by:

$$\sigma_M = \frac{PR_H}{2f} \text{ and } \sigma_H = \frac{PR_H}{2f}\left[2 - \frac{R_H}{R_M}\right] \tag{13}$$

where P is the inflation pressure, t is the material thickness, and R_M and R_H are the radii of curvature in the meridional and hoop directions. These are given by

$$R_M = 2f\left[1 + \frac{r^2}{4f^2}\right]^{3/2} \tag{14}$$

$$R_H = 2f\left[1 + \frac{r^2}{4f^2}\right]^{1/2} \tag{15}$$

where f is the focal length of the reflector, and r is the radius of a particular point on the reflector.

For the center of the paraboloid (minimum stress), r = 0, so that equations 14 and 15 reduce to

$$R_M = R_H = 2f \tag{16}$$

and equation 13 is reduced to

$$\sigma_M = \sigma_H = \frac{Pf}{t} \tag{17}$$

which can be solved for pressure:

$$P = \frac{\sigma_M t}{f} = \frac{\sigma_H t}{f} \tag{18}$$

For example, Kapton® of thickness 7.6 microns, a paraboloid focal length of 55.9 meters and a required film stress of 4.48 MPa would dictate a pressure of 0.5Pa.

4.4 INFLATANT SELECTION

A previous study (Reference 21) was performed to determine the optimum inflatant to be used in low pressure space structures. These called for the use of water vapor for the following reasons:

1. With its container, water is the lowest weight inflatant.
2. Water is inert.
3. Water has sufficient vapor pressure to stress the reflector film.
4. Water is inexpensive.

While other lighter weight gases (i.e., hydrogen and helium) have been considered, the problem lies in their containment. Helium must be kept colder than -401°F to be a liquid; the saturation temperature for hydrogen is even lower. Insulation and/or a cryogenic cooling system would add a very significant weight penalty and add to the complexity of the system. On the other hand, to contain these inflatants in their gas state would require large and heavy high pressure tanks.

Water, on the other hand, is kept in its liquid state at pressures below 7000Pa (1 psi) at temperatures below 300K. When make-up gas is required, the water tank can be exposed to the lower pressure reflector feed line, allowing some of the water to boil-off into the reflector. (The vapor pressure of the water is higher than the reflector inflatant pressure, so that the gas will flow.)

Water (like any liquid) does require heat to vaporize. There is enough energy contained in the water itself to provide this heat. The greatest loss of water occurs upon initial erection of the paraboloid and is on the order of 0.001kg (0.0022 lb.) At temperatures between 273K and 294°K, it takes only 1 Kilojoule (1 BTU) to vaporize the .001Kg (.0022 lb.) of water, which can easily come from the stored energy in the remaining water. For the previous reasons, water is chosen as the baseline inflatant for the inflated reflector.

4.5 LEAKAGE THROUGH HOLES

The reason for determining the growth in hole area vs. time is to calculate the amount of replacement gas necessary for the mission. The mass loss is computed by using the free-molecular-flow kinetic relation which dominates in very low pressure applications. Leakage occurs when a molecule randomly encounters an opening in the film. This type of flow dominates when the mean free path of the gas inside the reflector is much greater (10 times greater) than the diameter of the meteoroid-produced hole (this occurs in a rarefied gas). A calculation was made to determine the maximum pressure where free-molecular flow still holds.

The equation for mean-free path, λ, is:

$$\lambda = \frac{1}{\sqrt{2}\,\pi\sigma^2 n_i} \tag{19}$$

Where σ is the molecular diameter, and n_i is the molecular concentration:

$$n_i = \frac{N}{V} = \frac{N_o P}{RT} \tag{20}$$

where N is the number of molecules in a volume V, P is the inflation pressure, R is the universal gas constant, and T is the gas temperature.

Substituting Equation 20 into 19 and solving for pressure yields

$$P = \frac{RT}{\sqrt{2}\,\pi\,\sigma^2\,\lambda\,N_o} \tag{21}$$

For most gases, $\varsigma = 3 \times 10^{-8}$ cm (Reference 22). The temperature is taken as room temperature (293°K) and the mean free path is 10 times the hole size. The most prevalent hole size is in the range of 10 - 20 microns (15 microns average); therefore, the mean-free-path should be 150 microns maximum. Inputting the above parameters into Equation 21 yields a threshold pressure of 67.3Pa (0.0098 psi) for free-molecular flow to exist. For all the reflectors in this study, the pressure is below threshold, so the leakage follows free-molecular flow theory.

The equations which govern this type of flow come from Reference 23; the mass loss is given by:

$$\dot{m} = \frac{n_i\,M\,\bar{V}A}{4N_o} \tag{22}$$

$$\bar{V} = \sqrt{\frac{8\,RT}{\pi M}} \tag{23}$$

where

A = hole area in film

m = mass flow rate through hole

M = molecular weight of gas (for H_2O, M = 18.02)

n_i = molecular concentration (molecules/cm^3)

N_o = Avogadro's number (6.02×10^{23} molecules/mole)

R = universal gas constant (8.314 KJ/Kg-mol°K)

T = temperature of gas (293°K)

V = mean molecular velocity

The molecular concentration is calculated by Equation 20.

$$PV = NRT \tag{24}$$

Substitution of equations 20 and 23 into Equation 22 yields the mass loss per unit time:

$$\dot{m} = \frac{PA}{4}\sqrt{\frac{8M}{\pi RT}} \tag{25}$$

or in terms of total mass lost:

$$m = \frac{P}{4}\sqrt{\frac{8M}{\pi RT}}\int A(t)\,dt \qquad (26)$$

where A(t) is the hole area in the reflector as a function of time, t. To simplify the situation, it is obvious that the average hole area in the reflector is the final hole area divided by two. For lifetimes different from one year, the gas loss increases as the square of time. This is due to the fact that the gas is constantly leaking out, plus the fact that new holes are also being created.

4.6 SYMBOLS

A - hole area in inflatable (m^2)
C_p - specific heat of balloon material (Kcal/Kg °C)
D - hole diameter caused by meteoroid (microns)
d - particle diameter (microns)
E_k - kinetic energy of particle (N m)
E_{melt} - Energy required to melt material (N m)
f - focal length of paraboloid (m)
G_e - defocusing factor
h_{fusion} - latent heat of fusion (Kcal/Kg)
h_{melt} - energy required to raise film temperature and melt film (Kcal/Kg)
m - mass of particle (g)
$\dot{m}$ - mass flow rate of leaked gas (g/sec)
M - molecular weight of gas
N - flux of particles (Section 2.0)
N - number of molecules (Section 6.0)
N_o - avogadro's number (6.02×10^{23} molecules/g mol)
n_i - molecular concentration (molecules/cm^3)
P - paraboloid inflation pressure (Pa)
R - universal gas constant (8.314 KJ/kg-mol °K)
R_H - radius of curvature in hoop direction (m)
R_M - radius of curvature in meridian direction (m)
r - radius of a point on a paraboloid (m)
T - thickness of film material (microns)
T_{melt} - melting temperature of material (°K)
T_o - initial temperature of balloon film (°K)
t - time (sec)
V - velocity of a particle (km/sec) (Section 3.0)
V - volume of gas (m^3) (Section 6.0)
V - velocity of leaking gas (m/sec)
Vol_c - volume of an impact-produced crater (m^3)
λ - mean-free-path in gas (m)
σ - mean molecular diameter (m)
σ_H - stress in hoop direction (Pa)
σ_M - stress in meridian direction (Pa)
ρ_f - density of film material (g/cm^3)
ρ_m - density of particle (g/cm^3)

REFERENCES

1. Grossman, Gershon, Analysis of Loads on Rim Support of Off-Axis Inflatable Reflector, L'Garde Technical Report LTR-87-GG-041, December 1987. [To be published in the Journal of Aerospace Engineering (ASCE), January 1991.]

2. Section 2.2. Inflatable Structures Technology Program Phase II, Final Report, L'Garde Report Number LTR-89-DS-033, October 1989 (Restricted Distribution).

3. Durcanin, J. T., D. R. Chalmers, and J. T. Visentine, "The Definition of the LEO Environment and Its Effects on Materials", AIAA 22nd Thermophysics Conference, June 8-10, 1987, AIAA-87-1599.

4. NBS, Technical Note 1116, May 1980.

5. Schwinghamer, R. J., "Space Environmental Effects on Materials", NASA TM-78306, August 1980.

6. Wieczorek, Mark D., "Conductivity of Metal/Polymer Coated Fabrics", July 1988, L'Garde Technical Report LTR-88-MW027.

7. Veal, G. and Thomas, M., Highly Accurate Inflatable Reflectors Final Report, L'Garde, Inc. March 1984.

8. Veal, G., Highly Accurate Inflatable Reflectors - Phase II Final Report, L'Garde Publication Number LTR-86-GV-129, October 1986.

9. Werntz, Paul and Stutzman, Dr. Warren, Computation of Radiation Properties of a Three-Meter Inflatable Reflector Antenna Constructed by L'Garde, March 1990.

10. Coffee, Jr. Claude W., Walter E. Bressette, and Gerald M. Keating, Design of the NASA Lightweight Inflatable Satellites for the Determination of Atmospheric Density at Extreme Altitudes, NASA TN D-1243, April 1962.

11. Hughes New Release "Science/Scope", Aviation Week & Space Technology, February 18, 1980, p. 70.

12. Sweet, George E., An Experimental and Analytical Investigation of Balloon-Type Enclosures for Thermal Control of Satellites, NASA TN D-5230, June 1969.

13. M. Thomas, "Parabolic Antenna Temperature Code (PANT)", L'Garde Report LTR-80-MT-102, December 26, 1980.

14. Cour Palais, B., Meteoroid Environment Model - 1969: Near Earth to Lunar Surface, NASA Special Publication SP-8013, NASA Johnson Space Center, March 1969.

15. Taff, L. G., et al, "Low Altitude, One Centimeter, Space Debris Search at Lincoln Laboratory (M.I.T.) Experimental Test System," Advances in Space Research - 1984, Volume 5, No. 2, Pages 35-46, Permagon Press, New York, 1985.

16. Kessler, D. J. and Cour-Palais, B.G., "Collision Frequency of Artificial Satellites: The Creation of a Debris Belt, "J. Geophys. Res. 83 (A6), 2637-46, June 1, 1978.

17. Maiden, C.J., & McMillan, A.R., "An Investigation of the Protection Afforded a Spacecraft by a Thin Shield", AIAA Journal, Vol. 2, No. 11, 1964.

18. Inflatable Structures Technology Program Final Report, L'Garde Report Number LTR-88-DS-010, June 1988 (Restricted Distribution).

19. Cour-Palais, B., "Preliminary Hypervelocity Impact Calibration of Solar Max Thermal Blankets and Louvers", 17th Lunar and Planetary Science Conference Abstracts, Part 1, March 1986, Lunar and Planetary Institute, Houston.

20. Veal, G., Highly Accurate Inflatable Reflectors, Phase II Final Report, L'Garde, Inc., AFRPL-TR-86-089, Air Force Rocket Propulsion Laboratory, Edwards Air Force Base, CA, March 1987.

21. Friese, G., Inflatant Study, L'Garde Information Release #210, December 1980.

22. Weast, R. C., Handbook of Chemistry and Physics, Chemical Rubber Co., 60th Edition, Page F-211, 1980.

23. Thomas, M. and Friese, G. J., Pressurized Antennas for Space Radars, paper presented at the AIAA Sensor Systems for the 80's Conference, Colorado Springs, CO, December 2-4, 1980.

SPACE ENVIRONMENT BIBLIOGRAPHY

Banks, Bruce, et al, "Protection of Solar Array Blankets from Attack by LEO Atomic Oxygen," 18th IEEE Conference of Photovoltaic Specialists, Las Vegas, Oct. 21-25, 1985.

Banks, Bruce, et al, "Ion Beam Sputter Deposited Thin Film Coatings for Protection of Spacecraft Polymers in LEO," NASA TM-87051, Presented at 23rd Aerospace Science Meeting of IAA, Reno, January 14-17, 1985.

Banks, Bruce A. and Sharon K. Rutledge, "Low Earth Orbit Atomic Oxygen Simulation for Materials Durability Evaluation," 4th International Sym. on Spacecraft in the Space Environment, Tolouse, France, September 6-9, 1988.

Coulter, D. R., R. H. Liang, S. Y. Chung, K. O. Smith, A. Gupta, "O-Atom Degradation Mechanisms of Materials", Jet Propulsion Laboratory

Dursch, Harry W. and Carl L. Henricks, "Protective Coatings for Composite Tubes in Space Applications", in Advanced Material Technology 87, Sample Proceedings, Volume 32, April 6-9, 1987.

Gulino, Daniel A., "Solar Dynamic Concentrator Durability in Atomic Oxygen and Micrometeoroid Environments," J Spacecraft, 25, #3, P. 244-249, May/June 1988.

Jacobs, Steve, Johnson Space Center, Telephone Communication on the exterior surface of the radiators for the space station, February 1989.

Kurland, Richard M., et al, "Properties of Metalized Flexible Materials in the Space Environment," Report SAMSO TR-78-31, AD B024667L, January 1978.

Leger, L. et al, "Review of LEO Flight Experiments," NASA Johnson Space Center, Houston, Texas.

Meshishnek, M. J., W. K. Stuckey, et al, "Effects on Advanced Materials: Results of the STS-8 EOIM Experiment," Aerospace Corporation, Report SD-TR-87-34, 20 July 1987.

Rutledge, Sharon, et al, "An Evaluation of Candidate Oxidation Resistant Materials for Space Applications in LEO," Workshop on Atomic Oxygen Effects, Jet Propulsion Laboratory, Nov. 1986, NASA TM-100122.

Schwingbamer, R. J., "Space Environmental Effects on Materials", NASA TM-78306, August 1980.

Smith, Kevin A., "Evaluation of Oxygen Interaction with Materials (EOIM) - STS-8 Atomic Oxygen Effect", TRW Thermophysics Lab, Redondo Beach, CA.

Whitaker, A. F., et al, "Evaluation of Materials for High Performance Solar Arrays," NASA TP 1220, April 1978.

Zimcik, D. G. and C. A. Maag, "Results of Apparent Atomic Oxygen Reactions with Spacecraft Materials During Shuttle Flight STS-41G", J Spacecraft, 25, #2, P. 162-168.

REPORT DOCUMENTATION PAGE

Form Approved
OMB No. 0704-0188

1. AGENCY USE ONLY (Leave blank)	2. REPORT DATE	3. REPORT TYPE AND DATES COVERED
	January 1992	Contractor Report

4. TITLE AND SUBTITLE
Inflated Concepts for the Earth Science Geostationary Platform and an Associated Flight Experiment

5. FUNDING NUMBERS
C NAS1-18681
WU 506-59-41-01

6. AUTHOR(S)
G. Friese

7. PERFORMING ORGANIZATION NAME(S) AND ADDRESS(ES)
L'Garde, Inc.
15181 Woodlawn Avenue
Tustin, CA 92680

8. PERFORMING ORGANIZATION REPORT NUMBER
LTR-90-GF-010

9. SPONSORING/MONITORING AGENCY NAME(S) AND ADDRESS(ES)
National Aeronautics and Space Administration
Langley Research Center
Hampton, VA 23665-5225

10. SPONSORING/MONITORING AGENCY REPORT NUMBER
NASA CR-187580

11. SUPPLEMENTARY NOTES
Langley Technical Monitor: Thomas G. Campbell
Final Report

12a. DISTRIBUTION/AVAILABILITY STATEMENT
Unclassified - Unlimited

Subject Category 18

12b. DISTRIBUTION CODE

13. ABSTRACT *(Maximum 200 words)*

Large parabolic reflectors and solar concentrators are of great interest for microwave transmission, solar powered rockets, and Earth observations. Collector subsystems have been under slow development for about a decade. Inflated paraboloids have a great weight and package volume advantage over mechanically erected systems and, therefore, have been receiving greater attention recently.

The objective of this program was to produce a "conceptual definition of an experiment to assess in-space structural damping characteristics and effects of the space meteoroid environment upon structural integrity and service life of large inflatable structures." The flight experiment was to have been based upon an inflatable solar concentration, but much of that was being done on other programs. Therefore, to avoid redundancy, the Earth Science Geostationary Platform (ESGP) was selected as a focus mission for this experiment. Three major areas concerning inflatables were studied under this program; the ESGP reflector configuration, flight experiment, and meteoroids.

14. SUBJECT TERMS
Inflatable antennas
Remote sensing
Earth system science

15. NUMBER OF PAGES
74

16. PRICE CODE
A04

17. SECURITY CLASSIFICATION OF REPORT	18. SECURITY CLASSIFICATION OF THIS PAGE	19. SECURITY CLASSIFICATION OF ABSTRACT	20. LIMITATION OF ABSTRACT
Unclassified	Unclassified	Unclassified	